3-28-2017

Quantity Trumps Quality: Bayesian Statistical Accumulation Modeling Guides Radiocarbon Measurements to Construct a Chronology in Real-time

Devon Robert Firesinger
University of South Florida, firesinger@mail.usf.edu

Quantity Trumps Quality: Bayesian Statistical Accumulation Modeling Guides Radiocarbon Measurements to Construct a Chronology in Real-time

by

Devon Robert Firesinger

A thesis submitted in partial fulfillment
of the requirements for the degree of
Master of Science in Marine Science
with a concentration in Geological Oceanography
College of Marine Science
University of South Florida

Major Professor: Brad E. Rosenheim, Ph.D.
Julie N. Richey, Ph.D.
Ryan P. Moyer, Ph.D.

Date of Approval:
March 28th, 2017

Keywords: gas ion source, accelerator mass spectrometry, isotope dilution, foraminifera, Pigmy Basin

Acknowledgments

I express my sincere gratitude to my advisor Dr. Brad Rosenheim, for providing wisdom, patience, enthusiasm and expert advice throughout this project. I thank my thesis committee: Dr. Julie Richey and Dr. Ryan Moyer for their insight and guidance through this research.

The National Ocean Sciences Accelerator Mass Spectrometry Internship (Woods Hole Oceanographic Institution), and the Anne and Werner von Rosenstiel Endowed Fellowship (University of South Florida) provided funding support for this research. I thank the researchers and crew onboard the R/V Pelican (2013), GoMRI (Gulf of Mexico Research Initiative), and CARTHE (Consortium for the Advanced Research of the Transport of Hydrocarbons in the Environment) for collection of this core. Thank you to Mark Roberts, Josh Burton, Josh Hlavenka, and Anne Cruz for valuable comments and assistance in the laboratory. I acknowledge Chris Smith and Caitlin Reynolds for helpful instruction when core splitting and washing sediment. I thank the many people of the Paleo Lab at the College of Marine Science for inspiration, comments, and help in the lab including: Mitch Lemon, Bryan O'Malley, Erika Fridrik, Amelia Shevenell, Patrick Schwing, Ryan Venturelli, Cristina Subt, Imogen Brown, and Nicola Zenzola. I extend my appreciation to Ethan Goddard for providing valuable contributions to this project and promoting my development as a researcher.

Lastly, I thank my family for the encouragement to pursue a field that fascinates me. Your love and support helped me begin this journey.

Table of Contents

List of Tables

List of Figures

Abstract

The development of an accurate and precise geochronology is imperative to understanding archives containing information about Earth's past. Unable to date all intervals of an archive, researchers use methods of interpolation to approximate age between dates. Sections of the radiocarbon calibration curve can induce larger chronological uncertainty independent of instrumental precision, meaning even a precise date may carry inflated error in its calibration to a calendar age. Methods of interpolation range from step-wise linear regression to, most recently, Bayesian statistical models. These employ prior knowledge of accumulation rate to provide a more informed interpolation between neighboring dates. This study uses a Bayesian statistical accumulation model to inform non-sequential dating of a sediment core using a high-throughput gas-accepting accelerator mass spectrometer. Chronological uncertainty was iteratively improved but approached an asymptote due to a blend of calibration uncertainty, instrument error and sampling frequency. This novel method resulted in a superior chronology when compared to a traditional sediment core chronology with fewer, but more precise, dates from the same location. The high-resolution chronology was constructed for a gravity core from the Pigmy Basin with an overall 95% confidence age range of 360 years, unmatched by the previously established chronology of 460 years. This research reveals that a larger number of low-precision dates requires less interpolation, resulting in a more robust chronology than one based on fewer high-precision measurements necessitating a higher degree of age interpolation.

Chapter One: Introduction

1.1 Historic role of ^{14}C in paleoceanography

Radiocarbon (^{14}C) dating is a technique used in paleoceanography to determine the age of a geologic sample. Radiocarbon is naturally produced as neutrons generated from cosmic rays bombard nitrogen atoms in Earth's atmosphere, thereby ejecting a proton out of the nitrogen nucleus to create the radioisotope ^{14}C (Libby et al., 1949). Radiocarbon atoms rapidly oxidize to form $^{14}CO_2$ molecules, which living organisms incorporate and constantly replenish into their tissue through photosynthesis or by consuming material derived by photosynthesis (Libby et al., 1949). Once an organism dies the ^{14}C exchange with the atmosphere ceases to occur and the ^{14}C content decays at a predictable rate. Willard Libby calculated the half-life (time necessary to decay half of the original amount of a radionuclide) to be 5568 years. Subsequent research determined the real value to be about 5730 years, however the 5568 year half-life is still used to construct ^{14}C calibration curves. Initially, measurements revolved around the absence or presence of ^{14}C in methane derived from different sources. Researchers noticed presence of ^{14}C in sewage CH_4 and absence of ^{14}C in petroleum CH_4 using Geiger-Müller counters (Anderson et al., 1947; Libby, 1967). This launched a campaign to attempt more precise ^{14}C determinations to date material from the past, however many methodological breakthroughs and developments were required before accurate measurements could be made.

First it was essential to reduce the sample size as the initial Geiger-Müller counter measurements required 20 liters of $^{13}CH_4$-enriched methane derived from six hundred liters (~300 g) of biomethane (Anderson et al., 1947). Liquid scintillation counting replaced the Geiger

counter and used specific organic compounds or scintillators to fluoresce when exposed to ionized radiation. Scientists later employed a spectrometer to count fluorescent events or individual ^{14}C decays, the frequency of which is proportional to the ^{14}C content of the sample (Ring et al., 1980). Eventually methodology progressed to react CO_2 with lithium at high temperatures to produce lithium carbide and later C_2H_2 after hydrolysis (Barker, 1953). This era of liquid scintillation ^{14}C research decreased background by 84%, reduced sample size to 100 mg C, and extended the limit of detection to 32,000 years (Polach, 1969; Polach et al., 1972; Polach, 1987).

While early ^{14}C measurement focused on decay events, the employment of accelerator mass spectrometry (AMS) enabled quantification of all ^{14}C present in a sample. Whereas the age of AMS began in 1939 (Alvarez and Cornog, 1939), it was not considered for ^{14}C determination until Richard Muller theorized the potential for dating radioisotopes with longer half lives (Muller, 1977). The problem researchers encountered in applying AMS to ^{14}C dating was the ability to distinguish between ^{14}C and ^{14}N to produce accurate measurements. This issue was solved using an external ion source to produce C^- ions, thereby eliminating N background and greatly improving the ^{14}C limit of detection (Bennett et al., 1977; Nelson et al., 1977). Negative ions created a new problem, however, where ^{13}CH and ^{14}C were indistinguishable from one another, so the tandem accelerator was introduced to convert C^- to C^+ and effectively strip hydrides passing through the system. Accelerators greatly reduced the measurement time per sample (5-10 minutes) compared to the liquid scintillation counting measurement times (>48 hours). In addition to shorter measurement time, increasing efficiency of ion sources and improved dating techniques decreased sample mass requirement to less than 1.0 mg C (Pearson et al., 1998).

Abundant research exploring Earth's recent history has sustained the development and innovation to continuously improve ^{14}C quantification. The limit of ^{14}C radiometric dating extends to approximately 45,000-50,000 years, however compound-specific ^{14}C analysis (Shah and Pearson, 2007) and advancements in sample pretreatment and analytical techniques allow for dating of certain material up to 50,000-75,000 years old (Stuiver et al., 1978; Behre and van der Plicht, 1992; Bird et al., 2003). Whereas the physics of ^{14}C measurements has improved, methods for pretreatment of samples and standards have transformed alongside the instrumentation. The chemical manipulation of samples and standards before ^{14}C analysis introduce minute amounts of contaminant C into the sample, so efforts have been focused on minimization of blank C. Depending on the sample type, C may be isolated through oxidation in a stream of oxygen, reaction with CuO or through acid hydrolysis with H_3PO_4. Post oxidation, the gas is usually cryogenically purified to remove non-condensable gases, and re-combusted to remove other impurities such as sulfur compounds. Generally solid C (graphite) is used as a target for AMS analyses, permitting ^{14}C quantification of ultra-small (0.001-0.025 mg) graphite samples (Santos et al., 2010; Shah Walter et al., 2015). Graphite is produced through the Bosch reaction: CO_2 and H_2 are reacted at high temperature with a Co catalyst to produce solid C and H_2O. A blank correction is typically applied to unknown ^{14}C measurements after the AMS operator observes the variability of known reference standards (Santos et al., 2007; Santos et al., 2010). To decrease the effect of blank C introduced during sample handling, chemical pretreatment, graphitization, and combustion, researchers reduce surface areas that sample can contact, bake catalysts, prebake quartz tubes and other tools used in sample preparation (Santos et al., 2007).

Radiocarbon dating advances not only enable scientists to date older and smaller samples, but emergence of new instrumentation has created a range of analytical options depending on the instrument used, composition of the sample, and the precision required for the measurement. Similar to advances in liquid scintillation counting through the mid-1900's, recent work has sought to reduce sample handling and expedite through-put of gas samples directly into a microwave ion source (Roberts et al., 2013) or as a modified analysis in a cesium sputter source (Ruff et al., 2007; Synal et al., 2007; Burke et al., 2010; Longworth et al., 2013). The exploration of rapid dating methods has been beneficial to researchers as a form of reconnaissance dating. Less-precise dating is a less expensive method used to age dredged deep-water corals, assisting in identifying specimens within a target age range (McIntyre et al., 2011; Thiagarajan et al., 2013). More recently this rapid ^{14}C dating has been used to create radial chronologies through ooid cross-sections (Beaupré et al., 2015).

1.2 Treatment of ^{14}C dates and formation of a chronology

Often scientists aim to plot proxy data orthogonal to time. Paleoceanographic research relies on exploiting information archived in marine sediments to reconstruct conditions in Earth's oceans. Information about temperature, water chemistry, biology, interactions with land, and many other parameters are recorded indirectly, as proxies. Stable isotope ratios of carbonate foraminifera microfossils, for instance, can be utilized to determine ancient sea-surface temperature, circulation patterns, ice volume, and general climate trends. Although time is crucial to deciphering proxy records, measurements of time (dates) are often made with less frequency than other proxy measurements (e.g. stable isotopes or trace elements) in a chronological record. Several informed assumptions must be made regarding the age of the

material at deposition to frame an age model from date measurements in order to model the age of sediment between measured dates.

Interpreting geological archives such as sediment cores involves not only accurate dating, but also constructing a sound chronology. Despite the modern advances in ^{14}C dating, age models of geological archives should not be considered to be as robust as the radiometric dates they are comprised of (Blaauw, 2010). All chronological interpolations have statistical uncertainty associated with them, and treating interpolated age models as flawless can result in serious misinterpretation of results. Paleoenvironmental information can be recorded differently even amongst records deposited and collected in close geographic proximity within the same region (Blaauw, 2010). Sedimentological processes and chronological uncertainty may cause asynchronous proxy events to merge into a single phenomenon (Figure 1A), or create two events from a single proxy event (Figure 1B), introducing a problem when attempting to align cores from different sites (Blaauw, 2010; Törnqvist, 2015).

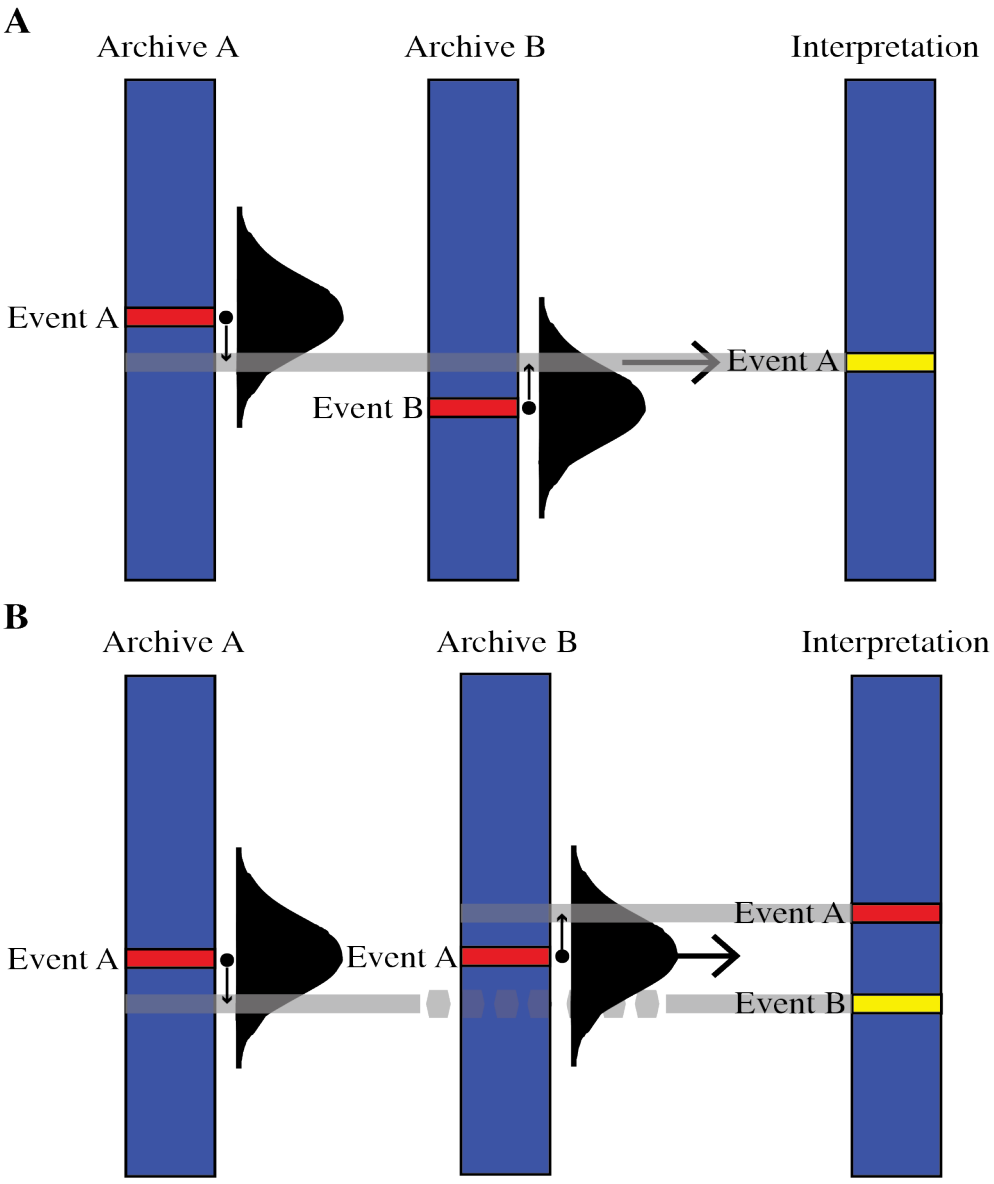

Figure 1: Proxy comparison among two archives illustrating the merging of two asynchronous proxy events into a single event (A), and the smearing of a single proxy event into two separate events (B) due to chronological uncertainty (black Gaussian curve) of radiometric measurements.

One must make several assumptions to frame ^{14}C dates into a chronology (Figure 2), for instance, when using marine samples, a reservoir age correction must be constrained for each specific sample. Atmospheric $^{14}CO_2$ molecules rapidly flux into the surface of the ocean, but there is exchange of water containing older (^{14}C depleted) dissolved inorganic carbon (DIC) between the deep-ocean and surface ocean DIC. Organisms incorporate DIC from the surface layer for primary production and for calcification of hard parts. An essential assumption must be made regarding the apparent age of material due to the blending of water masses. Dating material from open ocean settings is relatively predictable, the typical reservoir age correction for open ocean material is 400 years.

Material from certain water masses, high-latitude, freshwater, and coastal settings employ alternate reservoir corrections (Mangerud, 1972; Stuiver and Braziunas, 1993; Goodfriend and Flessa, 1997; Kennett et al., 1997; Ascough et al., 2009; Jones et al., 2010; Flower et al., 2011). In numerous high-latitude settings upwelling of ^{14}C depleted water masses mix with surface water, skewing the apparent age of the surface layer hundreds of years older than the standard 400 years. Rivers can supply water constantly shifting in reservoir age and error due to the presence, absence or blend of many carbon sources. This can cause a fluctuating reservoir age, making it difficult to form an accurate chronology in this type of setting.

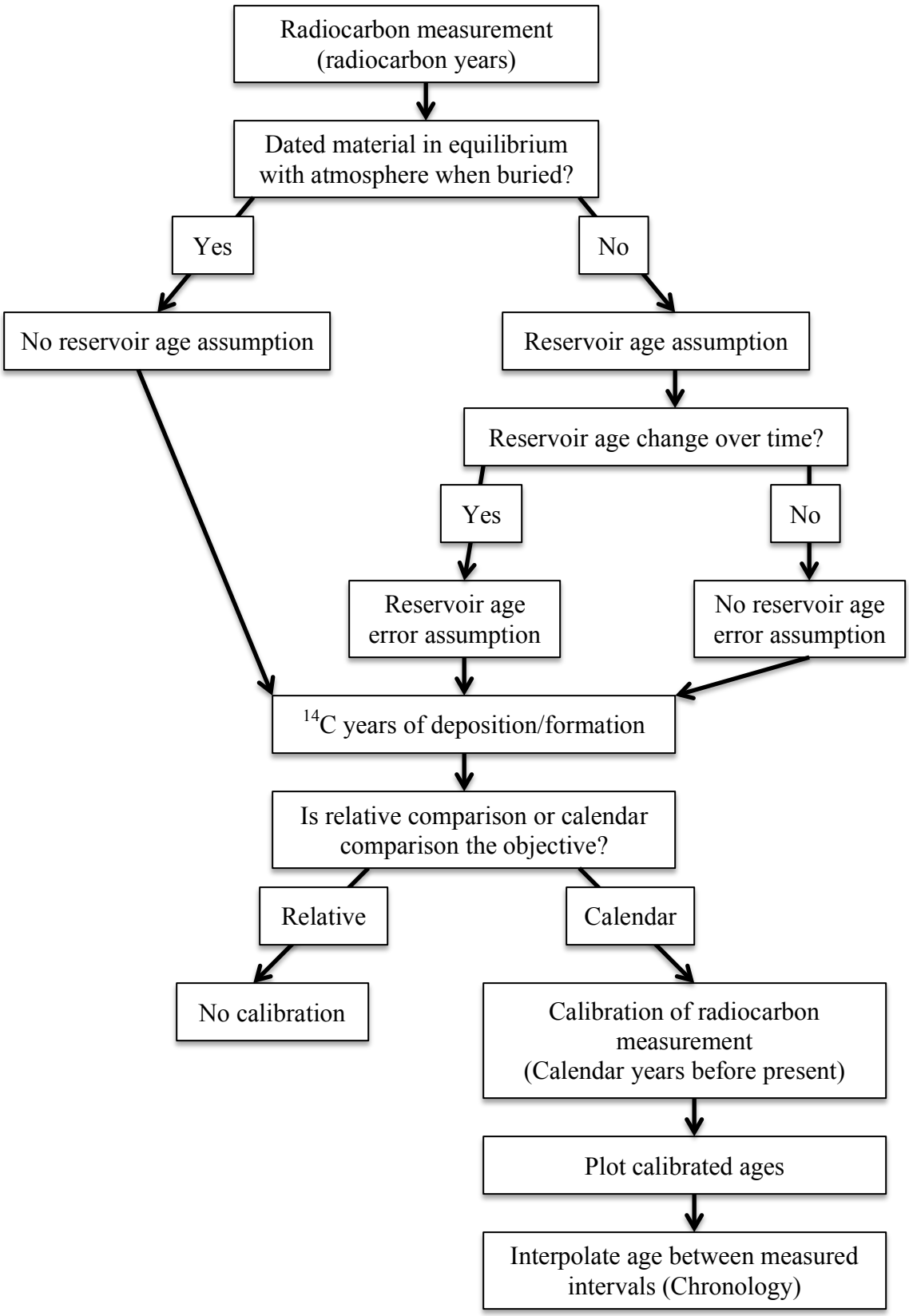

Figure 2: Flowchart of process to create a chronology beginning with a radiocarbon measurement.

A chronology interpolates through a series of dates. It is a tool which provides knowledge about the age and precision of when paleoenvironmental events, shifts, and other historical events occurred in the past. Before a specific date can be retained, one must explore the assumptions made to make this date acceptable. It is critical to understand the age variation of the ^{14}C pool where organisms are harvesting their carbon. Solar winds from the Sun and the Earth's magnetic field constantly change through time thus causing varying amounts of ^{14}C production in the atmosphere (de Vries, 1958). A primary goal of early ^{14}C research was to generate a calibration curve to characterize this natural variability and assist in the conversion from ^{14}C years to calendar years before present (cal. yr B.P.) (Klein et al., 1982). Calibration curves are engineered by measuring ^{14}C content of individual tree rings (Stuiver, 1982). Researchers selected long-living tree species (Irish Oak, German Oak, Douglas Fir, Sequoia and Bristlecone pine) employing both living and deceased specimens to create an overlapping chronology extending back to 12,400 calendar years Before Present (cal. yr B.P.) (Reimer et al., 2004). Uranium-thorium generated dates of corals and varved sediment from the Cariaco Basin extend the calibration curve further than dendrochronology permitted (Edwards et al., 1993; Bard et al., 1998; Burr et al., 1998; Hughen et al., 2004). The calibration curve has a well-defined slope leading to precise calibration in some areas (Figure 3). Certain sections of the calibration curve experience a change in natural production of ^{14}C such that the calibration slope becomes flat. This means a precise ^{14}C measurement (± 40 years) may carry a disproportionately large calibrated error (Figure 4) because a ^{14}C age located on a calibration curve plateau possesses an increased calibrated age range. Computer programs (e.g. Calib 7.10, OxCal) are available to calibrate ^{14}C dates (Stuiver and Reimer, 1986; Ramsey 1994; Stuiver et al., 2017) and even incorporate a calibration curve for marine samples (Hughen et al., 2004).

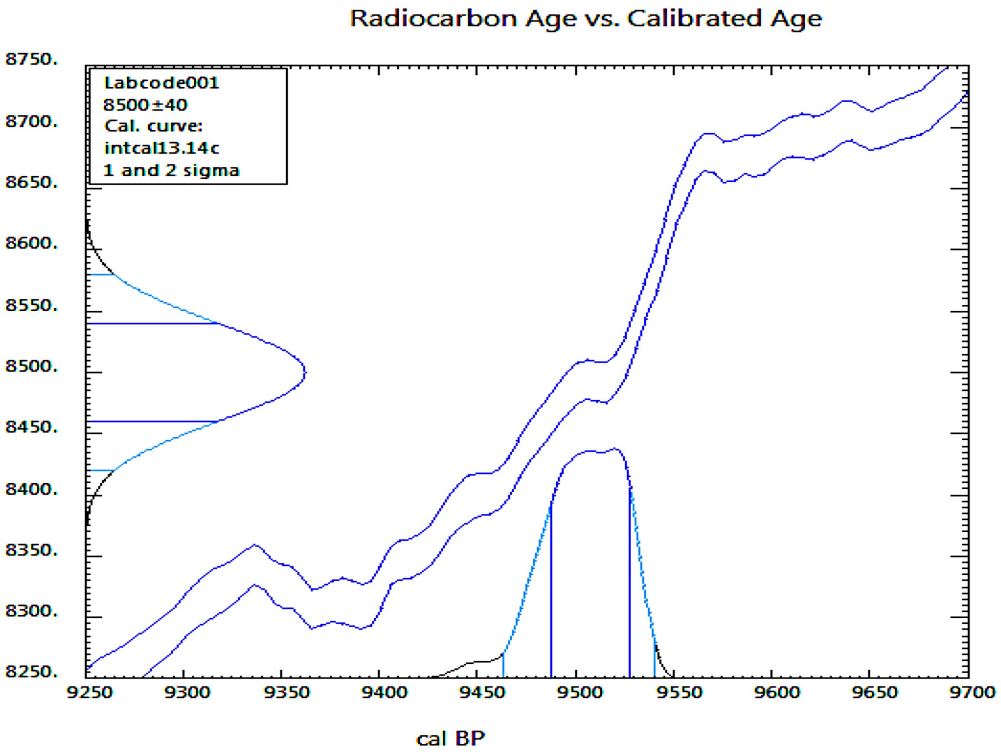

Figure 3: Slope of calibration curve when calibrating radiocarbon date 8500 ± 40 years (generated by the Calib 7.10 program, http://calib.org/calib/calib.html, Stuiver et al., 2017).

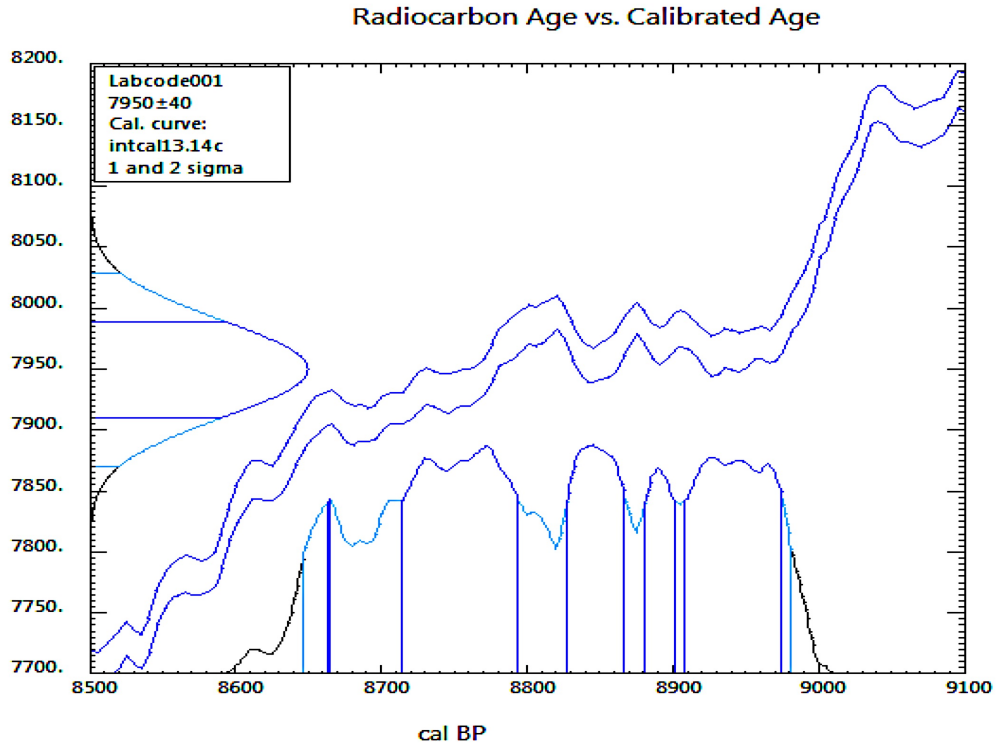

Figure 4: Slope of calibration curve when calibrating radiocarbon date 7950 ± 40 years (generated by the Calib 7.10 program, http://calib.org/calib/calib.html, Stuiver et al., 2017).

Many studies rely on fitting a linear or polynomial regression to interpolate the age of sediment between dated intervals of an archive. The model's accuracy is defended with an exceptional correlation of determination. Other research assumes that sedimentation is rarely consistent enough to assign a specific value spanning the entire record, so multiple accumulation rates or regressions are calculated to model the age between dates (Blaauw, 2010). The inability to date all intervals of the archive results in chronological interpolation between data points which is often unable to resolve high-frequency changes in accumulation rate. However, this resolution is necessary as accumulation rates fluctuate over time, as sedimentation rates adjust with glacial-interglacial oscillations, depositional sources, and/or geomorphological change.

Recently, a Bayesian statistical approach has been employed to model the accumulation of sediments. *A priori* assumptions are used to inform these statistical models to evaluate the relationship between neighboring dates and perform 'informed' interpolation between ^{14}C dates (Buck et al., 1991; Christen 1994). Analyses have applied Bayesian statistics to a group of radiometric ages to resolve the timing of a specific historical event with high chronologic precision (Egan et al., 2015; Sveinbjörnsdóttir et al., 2016). Several Bayesian statistical programs have been created which model ages between dates and reduce complications connected to the variance in accumulation rate over time (Christen, 1994; Ramsey, 2009; Blaauw, 2010; Blaauw and Christen, 2011; Nielsen et al., 2016). These Bayesian models follow the geologic law of superposition and often incorporate auxiliary tests to remove outliers, not meeting the prior assumptions of the Bayesian model (De Vleeschouwer and Parnell, 2014). This Bayesian approach has improved chronology production, reducing the range of possible calibrated ages by utilizing prior accumulation rate information and the relationship between neighboring dates.

More measured radiometric dates leads to less interpolation and a stronger chronology, however funding allocated to the age model is predetermined. This raises the question whether chronologies benefit more from precise dating and more interpolation, or less precise dating and less interpolation. This study uses a novel rapid Gas-Ion Source (GIS) AMS analyses to feed a Bayesian accumulation model to generate a ^{14}C chronology of equal accuracy and precision compared to a previous conventional graphitization ^{14}C chronology of a sediment core from the same area.

1.3 Geologic setting

The Pigmy Basin is a blocked-canyon intraslope basin located on the continental slope of the northern Gulf of Mexico (Figure 5). The basin is situated approximately 200 km south of the Mississippi River outflow. The DIC present in the vast marine reservoir is several orders of magnitude larger than the amount delivered by the Mississippi River into the Gulf of Mexico (Raymond et al., 2008). Pigmy Basin's distance is from the Mississippi river outflow, the dilution effect of riverine DIC with marine DIC, enhanced primary productivity at the outflow, suggest that minimal DIC from the Mississippi River reaches surface waters above Pigmy Basin. Sedimentation rates vary from about 43-80 cm/Ka during interglacial stages, to 300 cm/Ka throughout glacial periods (Richey et al., 2007; Montero-Serrano et al., 2009). The bulk of the sedimentation is attributed to the outflow of the Mississippi but this is mixed with material such as planktic foraminifera from the water column above. Positioned in an open ocean setting and receiving a high flux of sediments, Pigmy Basin supplies high-resolution archives to study scientific questions on a decadal to centennial scale. The extensive research performed on Pigmy Basin archives has investigated the sources and deposition of organic matter, routing of glacial meltwater, and climate variability in the northern Gulf of Mexico through the late Quaternary

(Jasper and Gagosian, 1990; Poore et al., 2004; Richey et al., 2007; Montero-Serrano et al., 2009, 2010; Poore et al., 2011; Richey et al., 2011). The Mississippi River contributes a substantial supply of hemipelagic material slowly transported to these continental shelf basins, however likely does not influence the reservoir age of certain material. Jasper and Gagosian conclude their 1990 paper by discussing an age offset between planktic foraminifera and sedimentary organic carbon ^{14}C dates. Foraminifera calcify from surface water DIC and sink vertically after death. Foraminifera represent the age of sedimentation better as the sedimentary organic carbon is transported great lateral distances and could originate from the erosion of old rocks upstream, or undergo severe aging before deposition (Jasper and Gagosian, 1990). To age correct ^{14}C data from organic matter the Ramped PyrOx method (Rosenheim et al., 2008) could be employed to produce ages from autochthonous material produced in the same setting as the planktic foraminifera and remove the age bias from allochothonous carbon. A chronology for a box core (MD02-2553) was developed to interpret proxies in previous literature (Poore et al., 2004, Montero-Serrano et al., 2009, 2010) providing an excellent scenario for comparison.

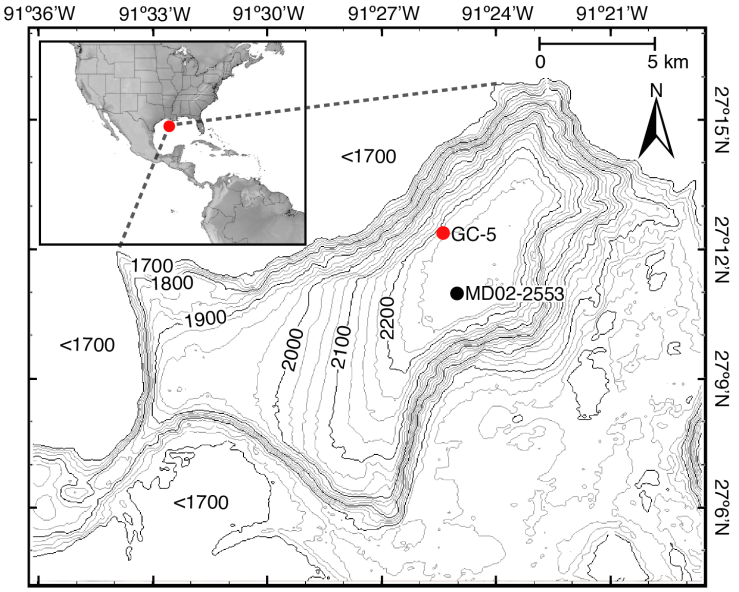

Figure 5: Map of the location of the Pigmy Basin (inset) and coarse bathymetry at the coring locations (Ryan et al., 2009, http://www.geomapapp.org).

Chapter Two

Preamble

Chapter two was prepared for publication in the journal *Geology*. Due to short formatting restrictions of this journal, a large portion of my research was not incorporated in this manuscript and will be covered in Chapter three.

Gas ion source accelerator mass spectrometry instructed by a Bayesian accumulation model to produce a radiocarbon age model in real-time

Devon R. Firesinger[1], Mark L. Roberts[2], Josh R. Burton[2], and Brad E. Rosenheim[1]

[1]College of Marine Science, University of South Florida, 140 7th Avenue South, St. Petersburg, Florida 33701, USA
[2]National Ocean Sciences Accelerator Mass Spectrometry facility, Woods Hole Oceanographic Institution, McLean Laboratory, Mail Stop #8, 266 Woods Hole Road, Woods Hole, Massachusetts 02543, USA

2.1 Scientific background

The establishment of a robust geological chronology is a cornerstone for any paleoclimate reconstruction, yet the number of age determinations applied to any chronology is necessarily finite. Regardless of the analytical precision of an age determination, the uncertainty in developing the chronology lies in the calibration to calendar age and interpolation over large intervals between age control points. Here, we demonstrate the advantageous combination of rapid, gas ion source ^{14}C determinations with a Bayesian statistical accumulation model to construct chronologies guided by statistical appraisal of the set of dates. A 280 cm gravity core recovered from the Pigmy Basin, Gulf of Mexico, was handpicked for >355 μm mixed planktic foraminifera every 3 cm down core for ^{14}C dating. The precision of the high-throughput date

determinations is reduced in our approach, but the Bayesian chronological models benefit more from quantity of dates than quality. The use of prior knowledge from the chronologic model to guide the sequence of what ultimately becomes an extremely dense set of dates outweighs the moderate increase in analytical error. The resultant high-quality chronology allows for better understanding of sediment accumulated in Pigmy basin throughout the majority of the Holocene and potentially revolutionizes chronologic approaches in geosciences to select for quantity in addition to quality.

2.2 Introduction

As new geologic archives are exploited to constrain Earth's history, improvements in our measurement of time are necessary to interpret and to compare the records. Chronologic models which interpolate between discrete age determinations have been developed to handle the ever-growing analytical precision of techniques such as ^{14}C dating. As computer power increases, conventional and over-simplistic chronological models employing interpolation (often linear) between individual dates has been supplanted by more sophisticated and computationally demanding *Monte Carlo* probabilistic techniques (Haslett and Parnell, 2008; Ramsey, 2009; Blaauw and Christen, 2011).

Recently, Bayesian statistical approaches have been employed, whereby *a priori* assumptions about the interrelationships of ages are used as guides for a statistical model to weight ages and to aid in the calibration of ^{14}C dates (Buck et al., 1991; Christen 1994). Analysts have applied Bayesian statistics to a group of radiometric ages to resolve the timing of a specific event (Egan et al., 2015; Sveinbjörnsdóttir et al., 2016), model the accumulation of sediments (Blaauw and Christen, 2011), and estimate the age of Greenland sharks (Nielsen et al., 2016). Several software packages (OxCal, Bchron, Bacon) have become available allowing

geoscientists to put dates into the framework of a Bayesian accumulation model (Haslett and Parnell, 2008; Ramsey, 2009; Blaauw and Christen, 2011). A simple *a priori* assumption is that material follows the geologic law of superposition and should get older as you move downcore. These models incorporate auxiliary statistical tests to remove outliers which do not meet the prior assumptions of the Bayesian model (Christen and Pérez, 2009; Ramsey, 2009). Bayesian chronologic models favor density of dates rather than high analytical precision of data, and can benefit from recently developed, low-cost, high-throughput, gas-ion source AMS methods. These techniques involve analysis of gas samples either directly (microwave ion source, Roberts et al., 2013) or as a hybrid analysis in a cesium sputter source (Ruff et al., 2007; Synal et al., 2007; Burke et al., 2010; McIntyre et al., 2011; Longworth et al., 2013). Both approaches yield quick turnaround, reduced sample handling, and high throughput, but generally a decrease in the precision of analyses. Thus they have been applied more for pre-screening and biogeochemical approaches than for chronologic applications.

However, these approaches offer the possibility to generate dense chronologic datasets that can strengthen Bayesian statistical accumulations models and allow detailed investigation of hiatuses, lithological changes, accumulation rate changes and instantaneous deposits such as slump events or turbidites. Here we run a Bayesian accumulation model in real-time to inform rapid non-sequential dating by GIS-AMS analyses. The chronologic model of the sediment core is iteratively rebuilt with each successive ^{14}C measurement, thereby informing where subsequent analyses can further improve the model. The speed of AMS measurements of gaseous samples combined with the increasing precision and accuracy of a densely populated Bayesian accumulation model result in a dense chronology of unsurpassed detail and utility. We focus on the Pigmy Basin, an important site that has produced high resolution sediment archives due to

relatively high accumulation rates. Previous research focused on chronicling meltwater from the Laurentide Ice Sheet (Flower et al., 2004; Montero-Serrano et al., 2009), reconstructing past sea surface hydrography and climate variability in the northern Gulf of Mexico during the Holocene (Jasper and Gagosian, 1990; Richey et al., 2007; Montero-Serrano et al., 2009, 2010, Richey et al., 2011). We use an established core chronology from a previously published study in the Pigmy Basin (Poore et al., 2004) for comparison. Our study is based on ^{14}C analyses performed on planktic foraminifera, but this general approach can be applied to myriad sample types introduced to the AMS as CO_2 gas including: organic matter, wood, other carbonate minerals (e.g. speleothems, bivalves).

2.3 Methods

The GC-5 core (27.20552ºN, 91.42280ºW; water depth 2236 m) collected from Pigmy Basin (Fig. 6D) consists of Holocene hemipelagic sediments, with fine-grained terrigenous material delivered via the Mississippi River and biogenic material from the water column above. For our ^{14}C dates, we handpicked a mixed assemblage of planktic foraminifera from the >355 µm size fraction at 3 cm intervals downcore. We were careful to avoid foraminiera that were visually altered by dissolution of diagenetic overgrowths. Species abundances of these handpicked intervals can be found in Chapter three; they differ from previous Pigmy Basin research (Kennett et al., 1985; Flower and Kennett, 1990; Poore et al., 2003, 2011), because only the >355 µm size fraction was counted. Preparation for ^{14}C determination consisted of suspension in methanol and ultrasonication to remove clays or detrital material. Radiocarbon was measured on the GIS-AMS system (Han et al., 2007; Von Reden et al., 2008; Von Reden et al., 2011; Roberts et al., 2013). Acquisition time on each sample was approximately five minutes. For normalization purposes, a standard reference material and either a blank or secondary

standard was measured after every 5th unknown. Radiocarbon reference materials used in this study can be found in Chapter three and the Appendix.

To maintain plasma stability in the first-generation GIS-AMS system a 25 mg mass of carbonate was required per analysis for ^{14}C determination, however 11-12 mg unknowns were also measured in this study. When measured, these small mass samples were not anomalous and consistent with the modeled chronology. Sampling of the core revealed lean intervals containing insufficient mass (<25 mg) of suitable >355 µm foraminifera for reliable measurements, necessitating other techniques to ensure oversampling of the core. Previous ^{14}C dating experiments have employed isotope dilution when there is insufficient dateable material (Gillespie et al., 1972; de Rooij et al., 2008) by supplementing unknown fraction modern (Fm) carbonate with a diluent carbonate of known Fm.

Fast and relatively inexpensive ^{14}C analyses allowed for an additional experiment to evaluate differences in the ^{14}C content of different calcareous sediment fractions. We compared bulk unsorted microfossil residues from two size fractions (>355 µm and 212-355 µm), handpicked mixed assemblages of planktic foraminifera from two size fractions (212-355 µm and >355 µm), and monospecific planktic foraminifera from the >355 µm fraction (*P. obliquiloculata, N. dutertrei*, and *G. truncatulinoides*). We also tested the efficiency of isotope dilution in rapid analysis chronologies such as this using samples of handpicked >355 µm mixed planktic foraminifera diluted with carbonate of known Fm. Lastly, we evaluated differences between GIS-AMS and ^{14}C dates measured by cesium sputter source on the >355 µm mixed assemblage foraminifera.

Radiocarbon ages were converted to calendar years B.P. by a Bayesian accumulation model (Bacon). We assumed a zero core-top age and a local marine reservoir age of 400 years

(ΔR=0) is assigned to age models to compensate for the age of the DIC pool in seawater (Stuiver et al., 1986). The associated reservoir age error (ΔSTD) was set to ± 10 years due to expected fluctuation over the length of the core. Meaning to compensate for the reservoir effect at this location, a 400 ± 10 year correction was applied to each date. Druffle and Williams created $\Delta^{14}C$ DIC depth profiles of the top 1000m in the Pacific, organisms may harness different aged DIC due to the stratification of water masses (Druffle and Williams, 1991). This data could be very helpful for chronologic work, however no such profile exists in the Gulf of Mexico at this time. Chronologic work in coastal settings, lakes, or ocean regions with variable reservoir ages would have to make different assumptions. Bacon averaged thousands of Markov Chain Monte Carlo iterations of the calibrated ^{14}C dates, calculating the 'best' model, the depths of minimum uncertainty, maximum uncertainty as well as a 95% confidence age range based on the weighted mean ages.

2.4 Results

Knowledge of the core depth with highest chronological uncertainty in the archive instructed each subsequent depth interval to quantify for ^{14}C. The Bacon chronology using four ^{14}C dates (95% confidence age range: 1359 years, Fig. 6A) is imprecise, however consecutive ^{14}C measurements iteratively reduced age uncertainty throughout the experiment. The final age model composed of 85 GIS-AMS and 10 cesium sputter source ^{14}C dates, reducing the 95% confidence range to 332 years (Fig. 6A). The Bacon student-t distribution disregarded a few outlying dates, which did not meet *a priori* assumptions of the model.

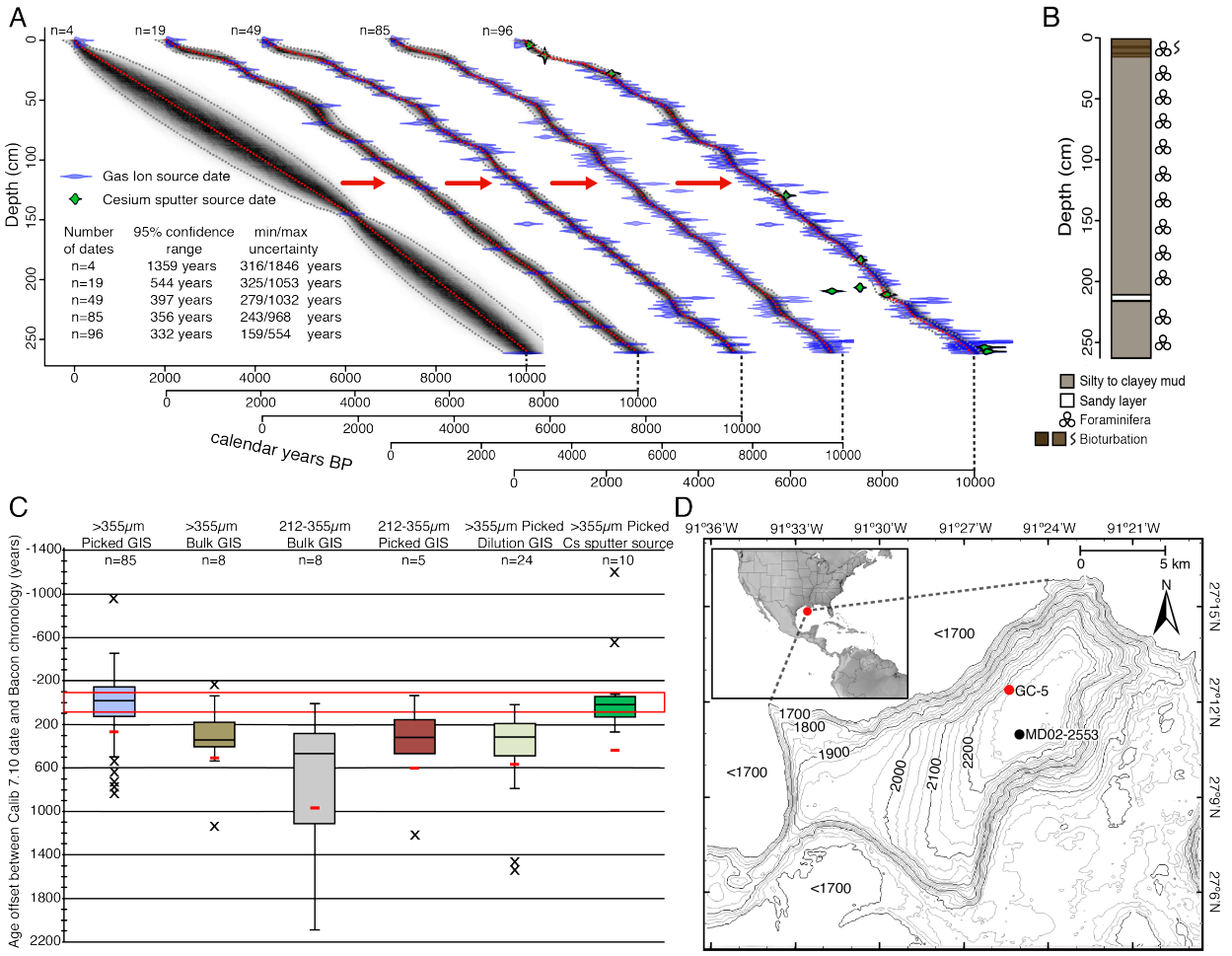

Figure 6: A) Evolution of Bacon-informed Gas Ion Source-Accelerator Mass Spectrometer (GIS-AMS) chronology showing increasing precision of accumulation model, GIS-AMS ^{14}C dates (blue), Cesium sputter source ^{14}C dates (green), grey dotted lines represent 95% confidence ranges and red dotted lines denotes the best model based on the weighted mean. The final chronology comprised of 85 GIS-AMS dates and 10 cesium sputter source dates, 332 year 95% confidence range. B) PE13-33-7 GC-5 core lithology diagram, indicating a hiatus ~213-215 cm. C) Comparison of chronometers at equivalent core depths, median age offsets of calibrated (Calib 7.10) dates compared to the weighted mean of the Bayesian Accumulation model chronology. Red rectangle illustrates average instrument uncertainty ± 89 years, root mean square error marked by red points, and outliers by black x points. D) Map of Pigmy Basin with coarse scale bathymetry (Ryan et al., 2009, http://www.geomapapp.org).

The establishment of a chronology permits comparison of individual calibrated ages (Calib 7.10) derived from different chronometers at equivalent core depths (Stuiver et al., 2017). The calibrated ^{14}C dates of >355 μm picked foraminifera (the main component to the age model) differed on average by 14 cal. yr B.P. (n=85) younger than the weighted mean age of the chronology at respective depths (Fig. 6C). This value is considerably lower than the GIS-AMS

average analytical uncertainty of ± 89 ^{14}C years, and much lower than calibrated age errors based on those dates. Conversely, the median calibrated age offsets were much larger for bulk material (unpicked) from both the >355 µm and the 212-355 µm size fractions (342 cal. yr B.P. (n=8) and 471 cal. yr B.P. (n=8) older, respectively). Also, the mixed planktic foraminifera picked from the 212-355 µm fraction and >355 µm isotope dilution were also older than the chronology (327 cal. yr B.P. (n=5) and 320 cal. yr B.P. (n=24), respectively). Cesium sputter source calibrated dates from >355 µm picked planktic foraminifera generate a median age offset of 29 cal. yr B.P. (n=10) older. For species-specific comparisons, *P. obliquiloculata* generate a younger calibrated age offset of 503 cal. yr B.P. (n=1), where *G. truncatulinoides* and *N. dutertrei* reported older age offsets of 275 cal. yr B.P. (n=2) and 182 cal. yr B.P. (n=2).

2.5 Discussion

Although our approach relied heavily on GIS-AMS ^{14}C dates, we also used conventional cesium sputter source AMS ^{14}C dates to initiate our process and to accommodate core depths where a paucity of foraminifera prevented oversampling. It is important to note that the 95% confidence age range of the Bacon chronology with 85 GIS-AMS dates improved by only 24 years with the addition of 10 cesium sputter source dates (Fig. 6A), however the maximum uncertainty was greatly reduced from 968 to 554 years. This was in large part due to the lack of dates, and hence control of the Bayesian model, at depths with coarse grains in the muddy matrix that contained significantly fewer foraminifera. Using only the 10 cesium sputter source ^{14}C dates, the 95% confidence range of the Bayesian chronology is 808 years. Excluding outlying dates from within the coarse-grained layer, the remaining 8 cesium sputter source dates produce an 816 year 95% confidence range, indicating these outliers did not greatly influence the model.

Operating under identical analytical cost, the less precise high frequency GIS dating technique produced a more constrained chronology for GC-5 compared to the MD02-2553 core chronology from previous research (Poore et al., 2004). We randomly generated chronologies from smaller subsets of the 85 GIS-AMS dates from GC-5, to compare with 16 cesium sputter source dates from MD02-2553, both assuming a zero core-top age. This dating density was selected to constrain archives that span the equivalent age and to have identical ^{14}C measurement cost and random numbers were applied to eliminate the bias of selecting ideal GC-5 dates. The 95% confidence range of the 75 date GC-5 chronology is 360 years, where the 16 cesium sputter source date MD02-2553 chronology is 466 years.

When coupling our dense data set with a Bayesian accumulation model, the resulting age model relies less on interpolation between discreet data points, resulting in better chronostratigraphic characterization of the archive. The chronology indicates Pigmy Basin has experienced a fairly consistent sediment accumulation rate throughout the middle to late Holocene, however age reversals and sedimentological information (Fig. 6B) indicate an unconformity early in the record (213-215 cm). The GIS-AMS chronological method enhances resolution around this sandy layer. Such details would have been lost if we had sampled with coarser resolution. This oversampling method could offer better chronological constraint of archives extracted from environments exhibiting considerable lithological change, substantial fluctuation in sedimentation rates or an abundance of hiatuses.

The ability to generate a dense ^{14}C data set allowed us to investigate what types of foraminifera, what size fractions, and what level of picking and cleaning compared well with the compiled chronology. To compare individual age determinations to the resulting chronology, ^{14}C ages of the former were calibrated using Calib 7.10 rather than the Bacon calibration routine.

Most individual dates are closer to the compiled Bacon chronology than average GIS-AMS instrument uncertainty (Fig. 6C). Radiocarbon content of unsorted sieved material represents planktic foraminifera of all sizes with a small portion of biogenic microfossils (e.g., benthic foraminifera, pteropods, radiolarians, coccolithophorids, sponge spicules, etc.) effecting dates interpreted from these measurements (>355 µm is older by 342 cal. yr B.P., and 212-355 µm by 471 cal. yr B.P.). The assemblage picked from the 212-355 µm fractions contained abundant shallow water planktic foraminifera species, which should produce a younger age compared to >355 µm picked analyses if the stratification of water masses supply DIC varying in ^{14}C content. The older ages of bulk material and the 212-355 µm picked fractions could be linked with redeposition, higher affinity to dissolution or diagenesis of the dated material (Berger and Piper 1972, Wycech et al., 2016). The few species-specific measurements suggest that the stratification of water masses can supply planktic foraminifera with DIC varying in ^{14}C composition (more detailed discussion in Chapter three). *P. obliquiloculata* and *N. dutertrei* are abundant below the seasonal thermocline at about 50-70 m and 50-150 m water depth, *G. truncatulinoides* begins life in shallow depths, but adults may continue to calcify deeper in the water column at 200-250 m (Ravelo and Fairbanks 1992; Farmer et al., 2007; Spear et al., 2011). The majority of the picked material consists of planktic foraminifera species which reside at or below the surface mixed layer, therefore it may be logical to assume an increased reservoir age value.

The >355 µm picked planktic foraminifera isotope dilution analyses could be biased older due to poor repeatability of the diluent material CORS (n=12, Fm = 1.1037 ± 0.0090‰), larger age error of isotope dilution measurements due to the conservative propagation of error associated with the dilution of unknowns. The >355 µm picked planktic foraminifera samples measured by cesium sputter source could be older due to an instrumental age offset or sub-

micrometer diagenesis of a few tests skewing the average age of the sample older than expected (Wycech et al., 2016). A small number of degraded tests will have a stronger ability to skew the age of a 1.0 mg sample compared to a 25.0 mg sample.

The GIS-AMS is not limited to carbonate material, but is suitable to analyze organic matter as well, offering the potential to reduce sample handling and preparation time. The Bacon modeling routine is not confined to age modeling in real time, but could also serve to improve existing work by constraining high age uncertainty chronologies with additional dates. Additional benefits include (1) incorporation of multiple calibration curves, which allows one to determine if stratigraphic concurrent chronometers exhibit a uniform age offset throughout the archive and (2) utilization of alternative dating methods that permit independent or fused chronologies from the same record (Enkin et al., 2013; Jazwa et al., 2013, Kosnik et al., 2015). Radiocarbon measurements provided in real time to determine each subsequent interval to be dated could have a high impact for future paleoceanographic and archeological research.

To execute this technique successfully one must have access to a computer with the processing power to run a Bayesian model between date measurements. It behooves one to oversample the geologic archive, as date density increases, interpolation and age uncertainty of the chronology decrease. It is necessary to have an introduction system such as a Gilson GX-271 Liquid handler, which can be programmed to introduce samples to the analytical instrument in a non-sequential order. If measuring organic material on the GIS-AMS, CO_2 should be pre-cleaned on a vacuum line as foreign compounds threaten the stability of the plasma and thus measurement precision.

2.6 Conclusions

Employing a Bayesian statistical accumulation model in real-time while measuring radiometric dates is ideal because it identifies weak points in the chronology where additional measurements could reduce age uncertainty in the geologic archive. An auxiliary benefit of running this model in real-time informs the user of age uncertainty constraint per sample, diminished returns indicate when to terminate analysis. The combination of revolutionary Bayesian models with state-of-the-art high-throughput instruments initiates a new direction when dating geologic archives. Researchers now have the capability to rapidly construct a strong chronology at competitive analytical costs compared to traditional graphitization, while retaining the ability to use higher precision dating at specific intervals as required.

2.7 Acknowledgements

This research was funded through the National Ocean Sciences Accelerator Mass Spectrometry (NOSAMS) Graduate Student Internship Program. The core was taken during an ocean-going expedition funded by the Gulf of Mexico Research Initiative (GOMRI) through the Consortium of Advanced Research on the Transport of Hydrocarbon in the Environment (CARTHE). We thank the crew of the R/V *Pelican* (PE-13-33) for a successful research cruise.

Chapter Three

3.1 Supplementary methods and results

Preamble

Chapter three contains more a more detailed methods, results, and discussion. Chapter two was prepared for submission to *Geology*, the majority of Chapter three will contribute to the supplementary material of the manuscript.

3.1.1 Core sampling

The gravity core PE13-33-7 GC-5 (27.20552ºN, 91.42280ºW; water depth 2236 m) collected from Pigmy Basin (Figure 7) consisted of Holocene hemipelagic fine-grained gray mud with occasional faint laminations and contained an abundance of foraminifera.

Core PE13-33-7 GC-5 was split at the U.S. Geological Survey in St. Petersburg, the working half used for this research, the other half preserved as an archive in the core repository at the University of South Florida, College of Marine Science. Grain-size analysis was performed at 10 cm intervals downcore using a Malvern Masterizer laser diffraction spectrometer. This core was primarily comprised of silt-sized material, with clay and sandy material representing the remainder. Sedimentation was fairly consistent throughout the length of the core; the exception of this stable sedimentation at approximately 213-215 cm where a layer with a high percentage of sand was present (Figure 8). Three other sections of the core (20.5-30.5 cm, 90.5 cm, and 220.5-225.5 cm) had noticeably increased abundance of clay material (>50 %).

Sediment was wet sieved (63 µm) with deionized water to remove clay and silt material. The washed material placed in a 40 ºC oven overnight to dry. Once dry, sediment was dry sieved, and separated into four size fractions: 63-150 µm, 150-212 µm, 212-355 µm and >355 µm (Figure 9). The >355 µm size fraction selectively handpicked for pristine planktic foraminifera (Figure 10) at 3-cm intervals downcore for ^{14}C determinations on the GIS-AMS at NOSAMS.

The majority of mixed planktic foraminifera assemblages picked included: *Globorotalia truncatulinoides, Pulleniatina obliquiloculata, Neogloborotalia dutertrei, Globorotalia menardii* and variations of this species *G. tumida* and *G. ungulata, Globigerinoides ruber* (pink and white variety)*, Orbulina universa, Globigerina siphonifera, Trilobatus sacculifer,* and *Globorotalia crassaformis*. Picked samples were identified for up to 300 individuals if possible to provide knowledge of the proportion of planktic species for each depth interval (Figure 11). Abundances differ from previous Pigmy Basin research (Kennett et al., 1985; Flower and Kennett, 1990; Poore et al., 2003, 2011), because only the >355 µm size fraction was counted.

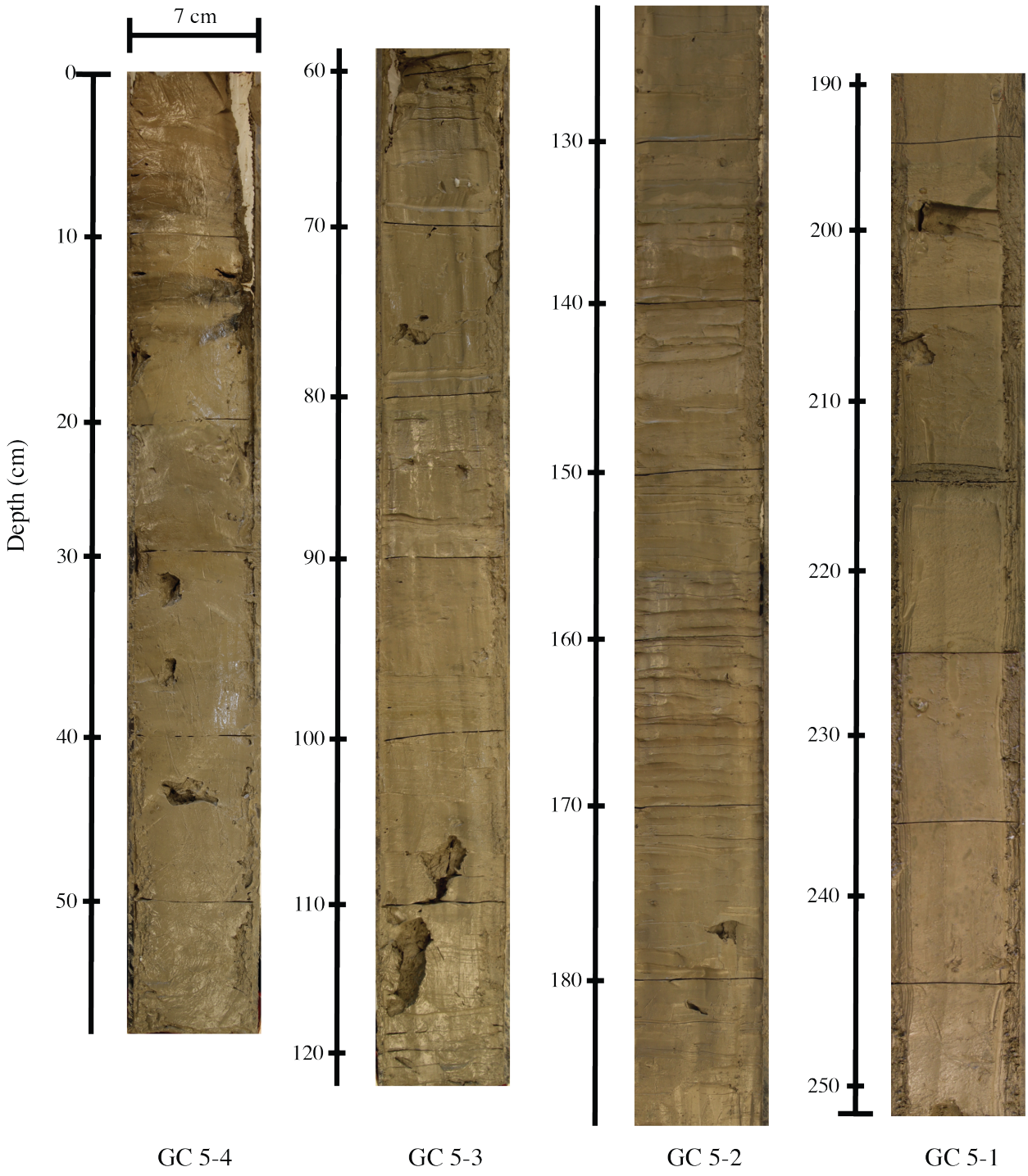

Figure 7: Photographs of the four PE13-33-7 gravity core sections.

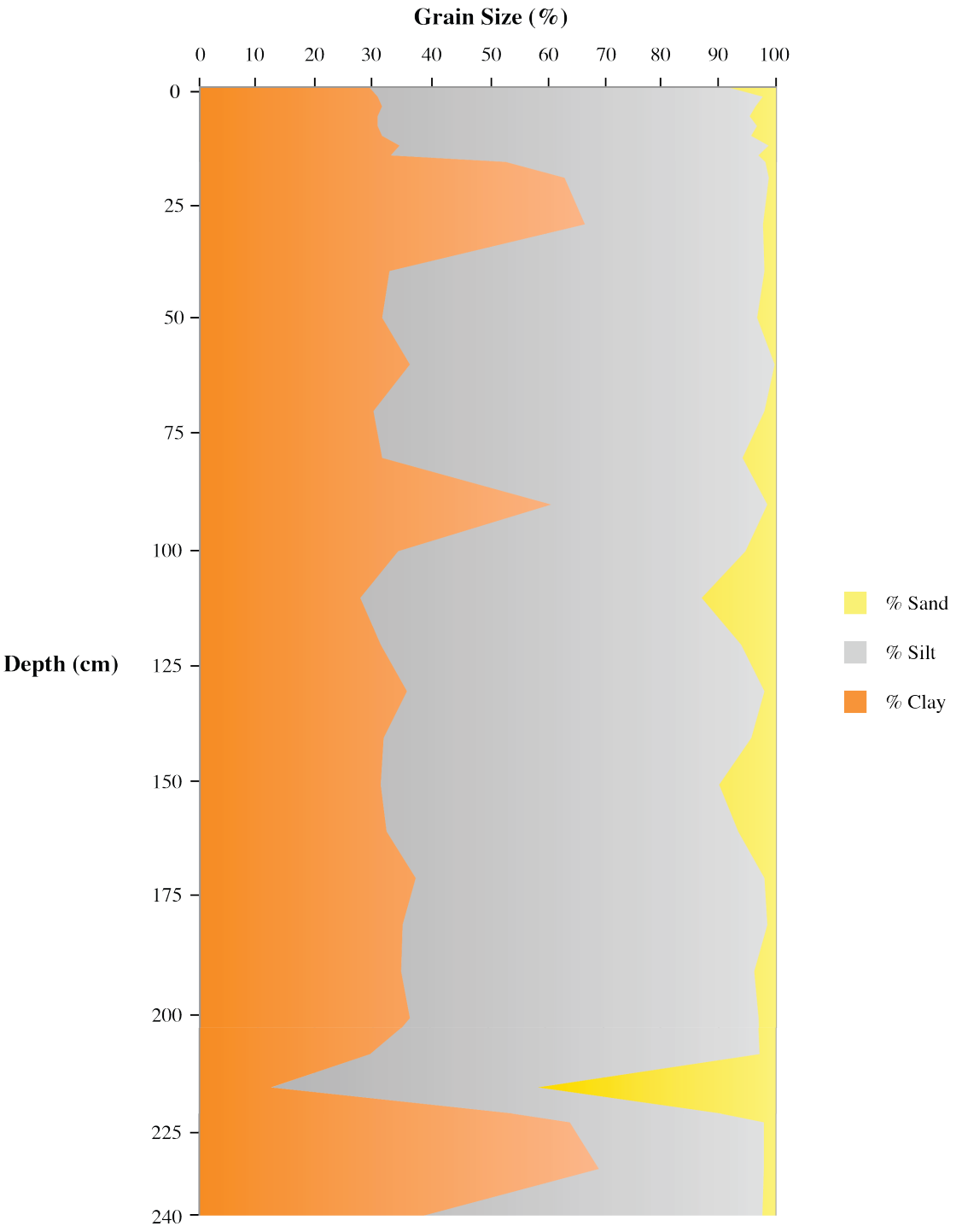

Figure 8: Grain size for core PE13-33-7 GC-5.

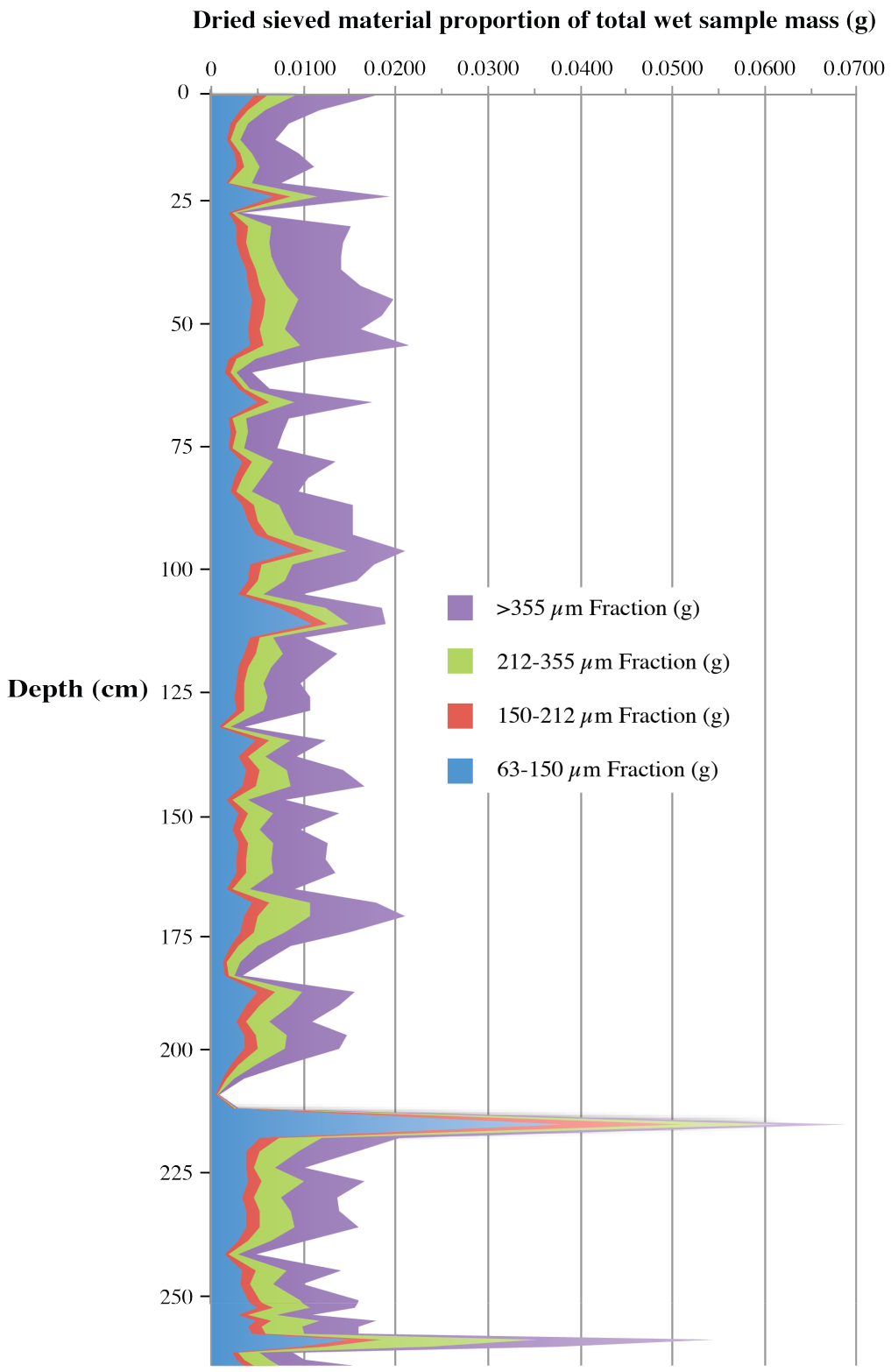

Figure 9: Mass of dried sieved fractions 63-150 µm (blue), 150-212 µm (red), 212-355 µm (green) and >355 µm (purple) from core PE13-33-7 GC-5.

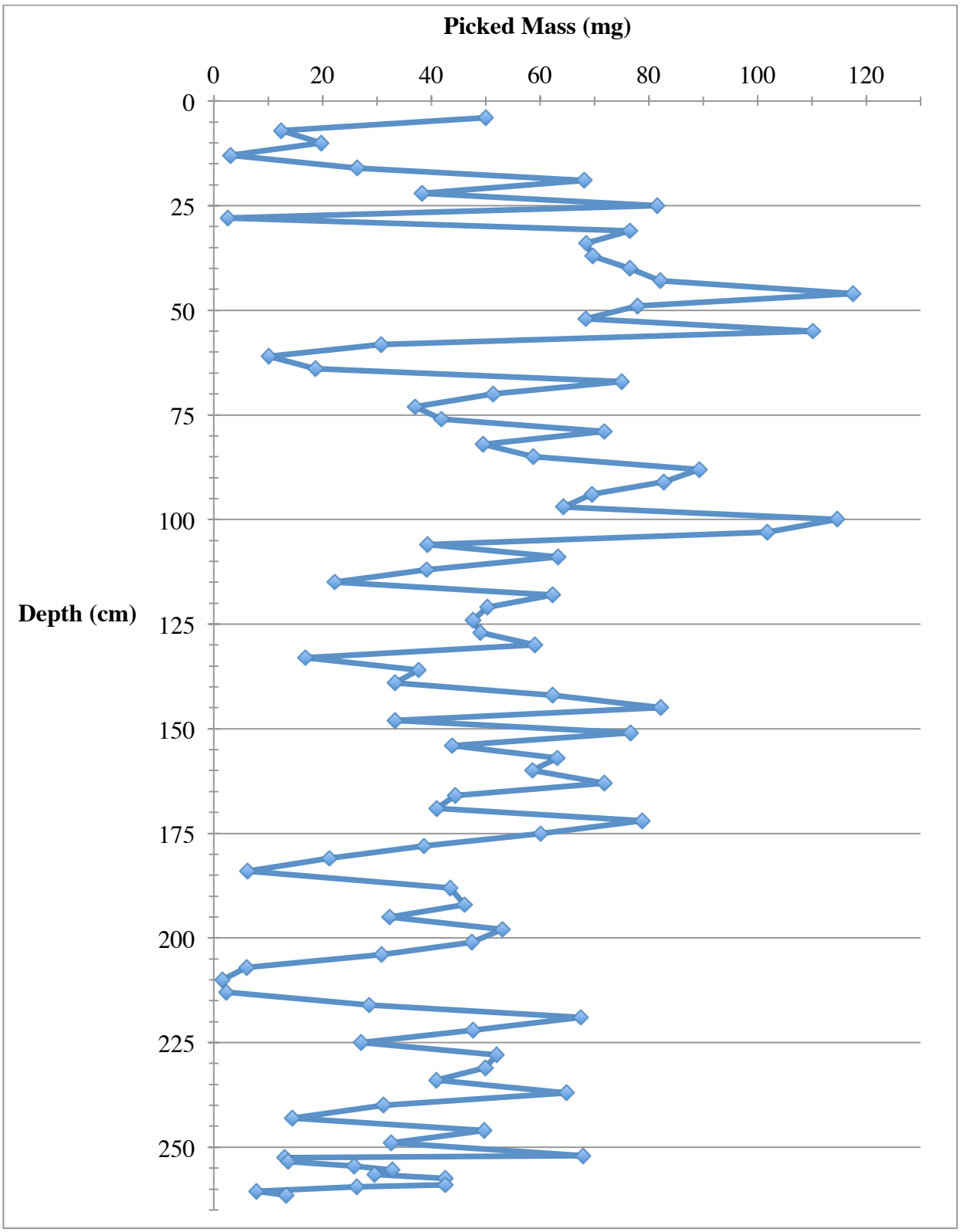

Figure 10: Mass of picked >355 µm planktic foraminifera from core PE13-33-7.

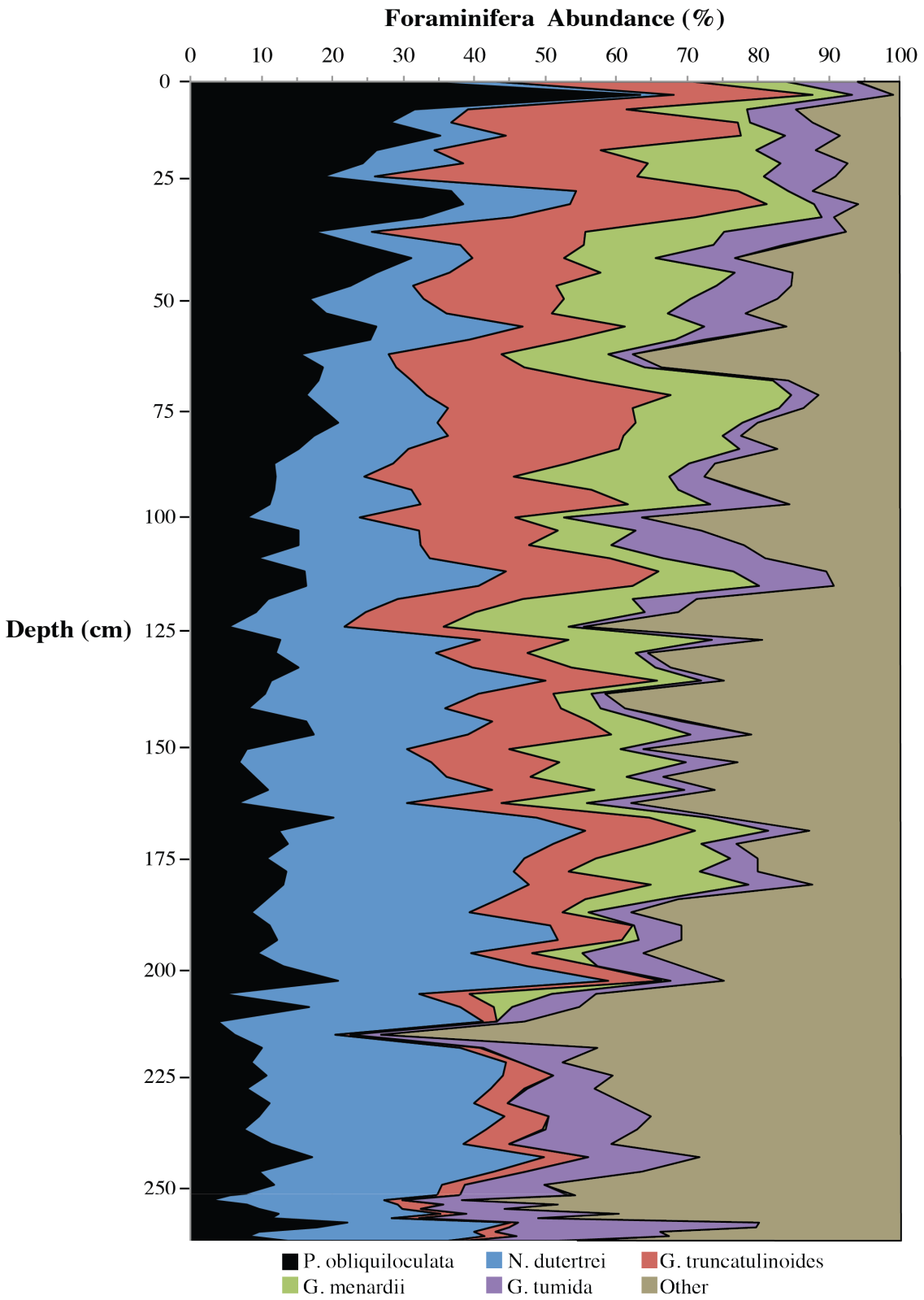

Figure 11: Relative abundances of >355 µm planktic foraminifera based on identification of 300 individuals if possible from core PE13-33-7 GC-5.

3.1.2 Carbonate ^{14}C analysis

Sample preparation consisted of suspension in methanol and ultrasonication to remove clays or detrital material. Radiocarbon was measured on the GIS-AMS system (Han et al., 2007; Von Reden et al., 2008; Von Reden et al., 2011; Roberts et al., 2013; Figure 12) coupled to a highly modified Gilson GX-271 Liquid handler (McIntyre et al., 2011; Roberts et al., 2013) at the National Ocean Sciences Accelerator Mass Spectrometry (NOSAMS) facility. Foraminifera were isolated in 7 mL Labco exetainer vials evacuated to ~10 mTorr, and reacted at a temperature of ~60 ºC, with 1 mL of 85% H_3PO_4 to produce CO_2 gas (Roberts et al., 2013). Complete reaction indicated when CO_2 bubbles ceased to form. Although cleaned foraminifera are not 100% $CaCO_3$, previous work has shown that phosphoric acid does not react with detrital organic matter to produce CO_2 (Roberts et al., 2013).

The beginning of each measurement series consisted of injecting modern reference gas into the ion source and optimizing system parameters. Then the Gilson Liquid handler was used to route a constant stream of CO_2 (~0.21 ml/min) from the vials through a ~3 m long capillary (inner diameter of 0.10 mm) to the source plasma chamber. Plasma was achieved using 2.45 GHz microwaves and an axial magnetic field. A low-energy bending magnet directed the resulting ion beam to the stripper canal of the accelerator. This component removed molecular interferences such as ^{13}CH and $^{12}CH_2$. After proceeding through the accelerator the beam was directed by a second high-energy bending magnet, ensuring that carbon isotopes were exclusively measured on the off-axis ^{12}C and ^{13}C faraday cups and the inline ^{14}C detector (Han et al., 2007; Von Reden et al., 2011).

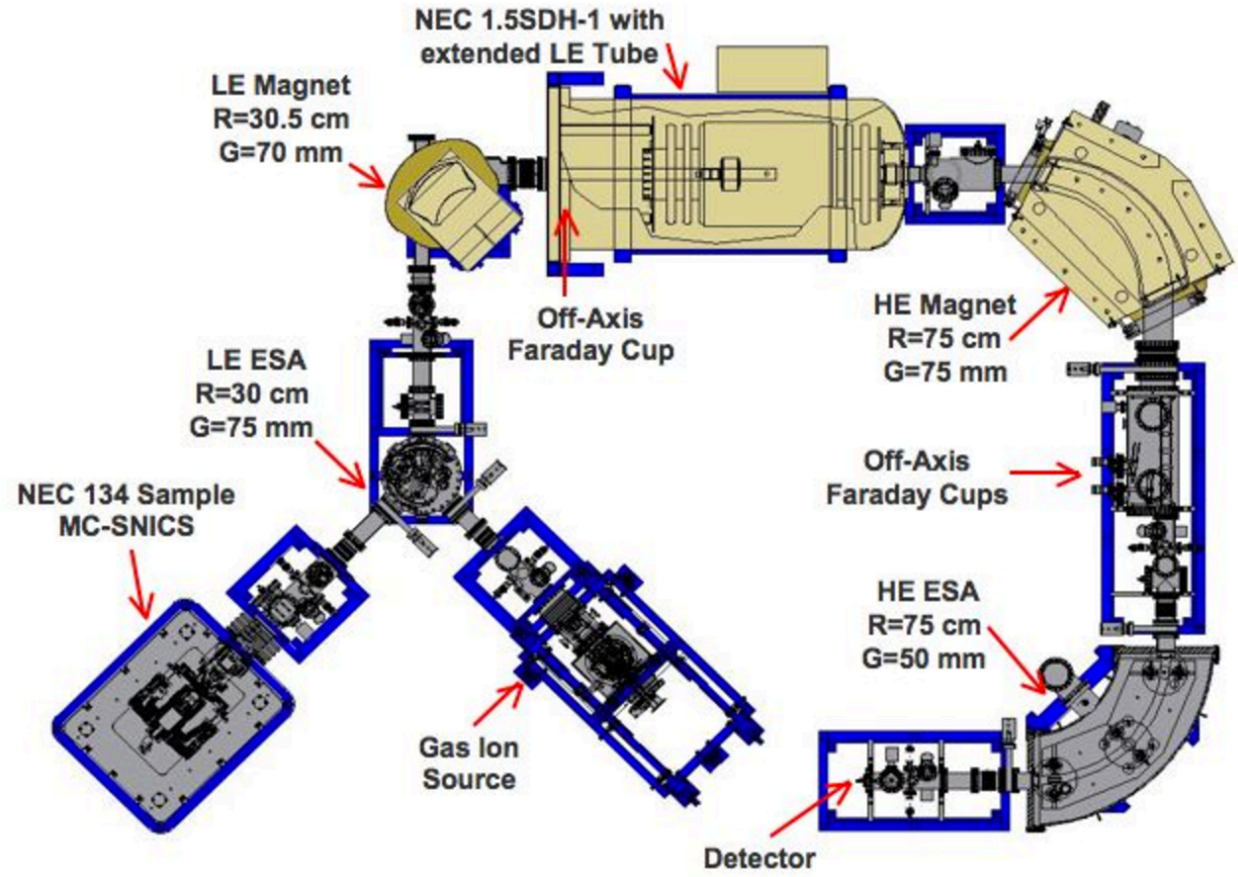

Figure 12: Schematic of the Gas Ion Source-Accelerator Mass Spectrometer system taken from the National Ocean Sciences Accelerator Mass Spectrometry website http://www.whoi.edu/nosams/page.do?pid=40149&tid=282&cid=74873.

Acquisition time on each sample was approximately five minutes. The first minute or two of data was not used to calculate Fm due to possible memory from the previous sample. The final three to four minutes of each signal peak in the data generated statistics, used to calculate Fm of the sample (Von Reden et al., 2008). By substituting values for the measured Fm (Fm), the background Fm (Fm_b), and the expected Fm (Fm_s) each sample was blank corrected according to Equation 1.

$$Equation\ 1 \qquad Fm_c = Fm - Fm_b \frac{Fm_s - Fm}{Fm_s}$$

The Fm, Fm_b, Fm_s, the measured Fm error ($Fm \pm$), and the background Fm error ($Fm_b \pm$) were used to propagate corrected Fm error ($Fm_c \pm$) (Equation 2).

$$Equation\ 2 \qquad Fm_c \pm = \sqrt{\left[\frac{1+Fm_b}{Fm_s}\right]^2 \left[Fm \pm\right]^2 + \left[\frac{Fm}{Fm_s - 1}\right]^2 \left[Fm_b \pm\right]^2}$$

The operator used $\delta^{13}C$ values from an in-line off-axis faraday cup to normalize Fm to -25 per mil $\delta^{13}C$ for samples and standards (Equation 3).

$$Equation\ 3 \qquad Fm_{\delta^{13}C} = Fm \cdot \left[\frac{(1-25/1000}{(1+\delta^{13}C/1000}\right]^2$$

The resulting corrected Fm was used to calculate the ^{14}C age (Equation 4).

$$Equation\ 4 \quad Age = -8033 \ln(Fm)$$

^{14}C reference materials used in this study include IAEA C1 marble, infinite ^{14}C age (0 ±0.002‰), IAEA C2 Travertine, 7135 ± 5 (0.4114 ± 0.0003‰) Rosenheim coral standard (CORS), (1.086 ± 0.006‰), and purified instrument grade CO_2 reference gas, (1.0398 ± 0.0006‰). The C1 standard was used for processing blank corrections. The CO_2 reference gas was used both as a normalizing standard and to evaluate the stability and repeatability of the system over the course of a run. C2 and CORS served as secondary standards (McIntyre et al., 2011). Long-term GIS-AMS measurement uncertainty is typically less than ±0.02‰ for $\delta^{14}C$.

The positive angle to large 25 mg sample size requested by the GIS-AMS system is that blank contamination is minimal, and minor improvement to the efficiency of the ion source can greatly reduce the mass requirement in the future. Sampling of the core revealed lean areas containing insufficient mass of pristine >355 µm foraminifera for reliable measurements, necessitating other techniques to ensure oversampling of the core. Previous ^{14}C dating experiments have employed isotope dilution when there is insufficient dateable material, diluting

unknown carbonate samples with a mass of carbonate with known Fm (Gillespie et al., 1972; de Rooij et al., 2008). Fast and relatively inexpensive ^{14}C analyses allowed comparison between the ^{14}C content of bulk unsorted fractions (>355 μm, 212-355 μm), handpicked mixed planktic foraminifera (>355 μm, 212-355 μm), handpicked monospecific species (>355 μm), and isotope dilution samples of handpicked >355 μm foraminifera to determine if they were useful in rapid-analysis chronologies such as this. A few areas of the core contained insufficient mass to measure on the GIS-AMS, these samples (>355 μm foraminifera) were measured by cesium sputter source.

3.1.3 Species-specific carbonate ^{14}C analysis

Scientific studies frame chronologies based on ^{14}C measurements from specific species of foraminifera, where others use mixed assemblages of foraminifera to measure ^{14}C content. Foraminifera display $\delta^{13}C$ variability due to precipitation depth and species vital effects, this variance not completely manifested to $\Delta^{14}C$ (Beger et al., 1978; Spero et al., 1991). Broecker et al., suggest *T. sacculifer* and *G. ruber* are more fragile foraminifera species prone to breaking or dissolution compared the sturdier robust *N. dutertrei* and *P. obliuiloculata*. If paired ^{14}C analyses of robust foraminifera are significantly older than the fragile foraminifera of same depth, this indicates presence of reworked material (Broecker et al., 2006). A suite of species-specific (*G. truncatulnoides, P. obliquiloculata,* and *N. dutertrei*) samples from several depth horizons were prepared for the GIS-AMS to identify if species-specific measurements yield age variation or lower age uncertainties compared to the mixed species analyses.

3.1.4 Isotope dilution carbonate ^{14}C analysis

Isotope dilution could help alleviate the substantial sample size required because not all intervals from sedimentary archives possess 25 mg of dateable material. A series of equations

were implemented in an effort to predict the error associated with diluting the unknown sample with a carbonate standard of known Fm. A binary mixing model uses Fm values of the unknown sample (δ_{Sam}), known diluent (δ_{Dil}) and associated concentrations (f) to calculate the theoretical measured Fm (δ_{Meas}) by the GIS-AMS system (Equation 5).

Equation 5
$$\delta_{Meas} = f \cdot \delta_{Dil} + (1 - f)\delta_{Sam}$$

This binary mixing model equation was manipulated to solve for δ_{Sam} (Equation 6).

Equation 6
$$\delta_{Sam} = \frac{\delta_{Meas} - \delta_{Dil}}{f} + \delta_{Dil}$$

Equation 5 was then substituted into an error propagation equation (Equation 7).

Equation 7
$$\sigma^2_{\delta_{Sam}} = \sum_{i=1} \sigma_{xi} \left(\frac{\partial y}{\partial xi} \right)^2$$

The resulting equation was simplified in order to propagate the errors involved with the dilution (Equation 8).

Equation 8
$$\sigma_{\delta_{Sam}} = \sqrt{\left[\frac{\sigma^2_{\delta Meas}}{f^2} \right] + \left[\frac{\sigma^2_f ((\delta_{Dil}(1-f)) - (\delta_{Meas}(f)))^2}{f^4} \right] + \left[\frac{\sigma^2_{\delta Dil}}{f^2} \right]}$$

Application of this set of equations revealed that a ^{14}C standard (Rosenheim CORS, Fm= 1.086 ± 0.006) should be utilized for the isotope dilution of selected core intervals. The age uncertainty was minimal <200 yr when measuring samples with high Fm content and the majority of the sample fraction from the unknown rather than the CORS standard. Age uncertainty became greater when less than 70% (17.5 mg) of the sample mass comes from the unknown material (Figure 13).

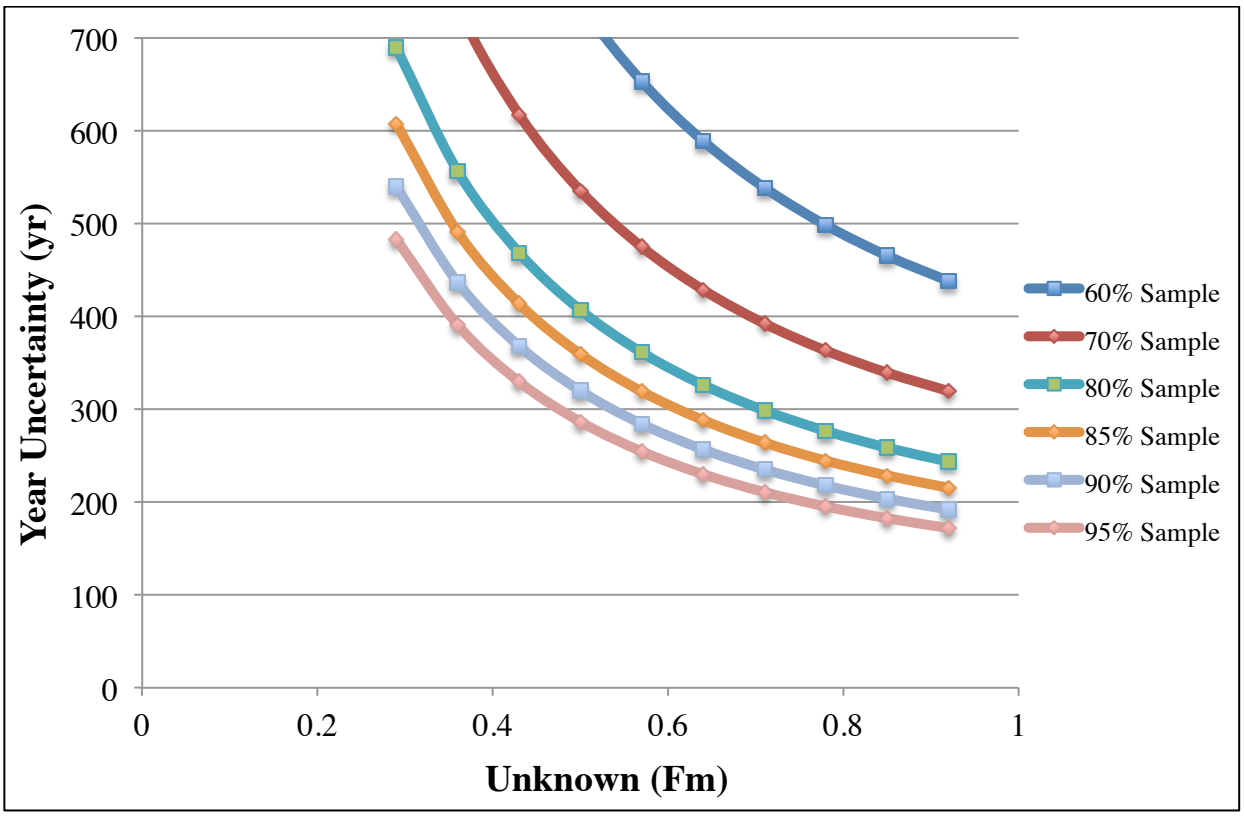

Figure 13: Age uncertainty calculated from assigned fraction modern values for the Unknown material. Different color markers utilized to represent the unknown/standard composition of the sample.

3.1.5 Bayesian accumulation model

Radiocarbon ages were converted to calendar years B.P. by Bacon however other software packages (OxCal and Bchron) exist, which can be employed instead of the Bacon program. We assumed a zero core top age and employed a reservoir age of 400 ($\Delta R=0$) ± 10 years as discussed in Chapter two. Bacon averaged thousands of Markov Chain Monte Carlo iterations of the calibrated ^{14}C dates, calculating the 'best' model, the depths of minimum uncertainty, maximum uncertainty as well as a 95% confidence age range based on the weighted mean ages.

The Bayesian accumulation model is a non-deterministic model. The operation window displays the age model and three other pertinent windows (Figure 14). The first is the log of

objective (Figure 14A), which allows the operator to gauge the strength of the age model. A strong run displays a stationary distribution but iterations possess little structure. The second accumulation rate window (Figure 14B) presents the prior accumulation rate in a green curve and the posterior accumulation rate in grey histograms. The memory panel (Figure 14C) can be left at default or modified by the operator to a number between 0 (no memory), and 1 (highly constant accumulation). The bottom window (Figure 14D) displays the best model (red dotted line) based on the weighted mean ages produced by averaging thousands of Markov Chain Monte Carlo iterations of the calibrated ^{14}C dates (blue). The grey dotted lines on either side of the red dotted line represent 95% confidence intervals.

Although previous research indicates that Pigmy Basin has experienced relatively consistent sedimentation over the Holocene and higher values could be assumed, the memory was left at the default Bacon setting (memory strength = 4, memory mean = 0.7). Bacon divided the core into 52 sections each 5-cm thick, modeling the accumulation rate for each section to produce the age-depth model.

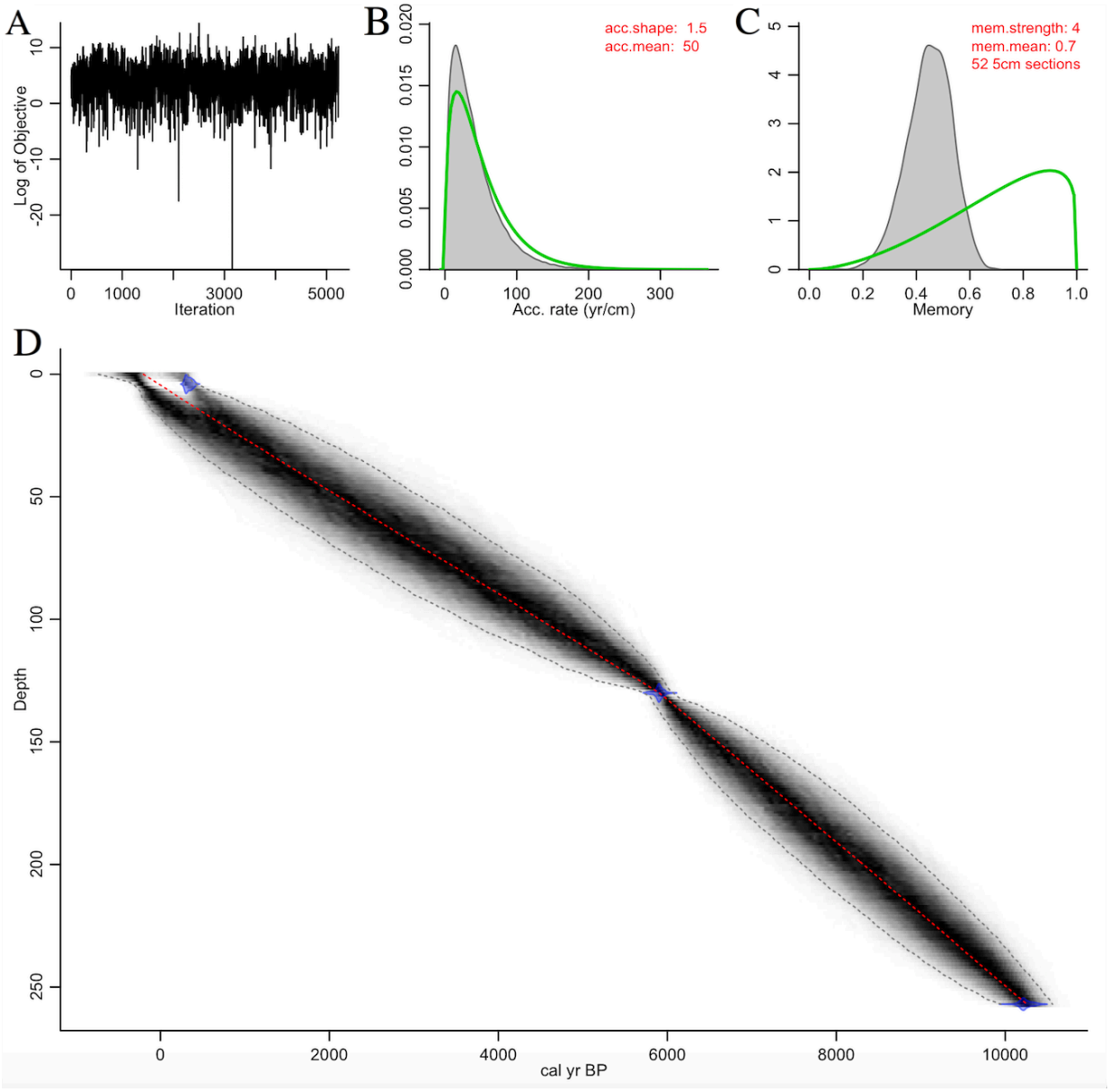

Figure 14: The Bacon output window. A) Log of objective to Markov Chain Monte Carlo iteration graph. B) Accumulation rate graph. C) Memory graph. D) Age model.

3.1.6 $\delta^{13}C$ and $\delta^{18}O$ stable isotope analysis

T. sacculifer and *G. menardii* assemblages were picked at 12-cm intervals from PE 13-33-7 GC-5. The >355 µm were picked from intervals for carbonate $\delta^{13}C$ and $\delta^{18}O$ analyses by a ThermoFisher MAT253 stable isotope ratio mass spectrometer coupled to a GasBench-II peripheral in continuous-flow mode at the University of South Florida College of Marine Science

Stable Isotope Biogeochemistry Lab. Larger assemblages of near similar size were utilized due to potential vital effects of individuals displaying $\delta^{13}C$ variability based on test size (Beger et al., 1978; Spero et al., 1991; Elderfield et al., 2002; Richey et al., 2012). Each sample was crushed, suspended in methanol and ultrasonicated to remove detrital material. Samples were reacted with phosphoric acid, and measured followed previously established procedures (Révész and Landwehr, 2002; Spötl and Vennemann, 2003; Duhr and Hilbert, 2004; and Burman et al, 2005). Secondary reference materials (TSF-1 $\delta^{13}C$ = 1.95±0.05‰, $\delta^{18}O$ =-2.20±0.06‰; Borba $\delta^{13}C$ = 2.87±0.05‰, $\delta^{18}O$ =-6.15±0.09‰, both calibrated to NBS19, NBS18 and LSVEC ($\delta^{13}C$ only) certified reference materials) were used to normalize measurements to the VPDB standard (Coplen et al., 2006). Measurement uncertainty, expressed as ±1 standard deviation of n=6 measurements of the TSF-1 laboratory reference material was ±0.02‰ and ±0.03‰ for $\delta^{13}C$ and $\delta^{18}O$ respectively. Long-term uncertainty measured by this machine is ±0.04‰ and ±0.06‰ for $\delta^{13}C$ and $\delta^{18}O$. Isotope ratio values are expressed in $\delta‰ = (R_{sample}/R_{standard})-1$, where R is the measured ratio of $^{18}O/^{16}O$ or $^{13}C/^{12}C$ (Coplen, 2011).

3.2 Supplementary results

3.2.1 Chronometer comparison by depth

In Chapter two the age offset between two different calibrations among several chronometers was explored. This chapter used the Calib 7.10 calibration program, to examine the age difference and calibrated error of the material being dated (Stuiver et al., 2017). Depth intervals displayed both similar and diverse ages among chronometers of equivalent depth (Figures 15-18). 31.0 cm, 55.0 cm and 88.0 cm give repeatable ages for material of different size, species, preparation method, and unknown dilution. Chronometers from 4.0 cm, 25.0 cm, 145.0 cm, 169.0 cm, 172.0 cm, 216.0 cm and 252.0 cm depth intervals give more variable ages. 121.0

cm, 151.0 cm and 252.0 cm possessed similar ages with the exception of >355 µm picked replicates and the isotope dilution measurement.

The >355 µm picked age at each depth was used for comparison purposes, if two >355 µm picked ages were present at a given depth, the age closer to the Bacon weighted mean was used instead of an average in an attempt to avoid bias from outlying dates. Unsorted material from the 212-355 µm fraction averages 530 calibrated years B.P. older than that of the >355 µm picked age, where the unsorted material from the >355 µm averaged approximately 150 calibrated years B.P. older. The 212-355 µm picked samples averaged 195 years older than the >355 µm picked samples of equivalent depth. The dilutions not only possessed a much higher average age of approximately 395 years, but also substantially inflated age error due to the conservative propagation of error. *G. truncatulnoides, and N. dutertrei* produced ages 220 and 145 calibrated years B.P. older, where the *P. obliquiloculata* measured 170 calibrated years B.P. younger than the >355 µm picked foraminifera from the identical depths.

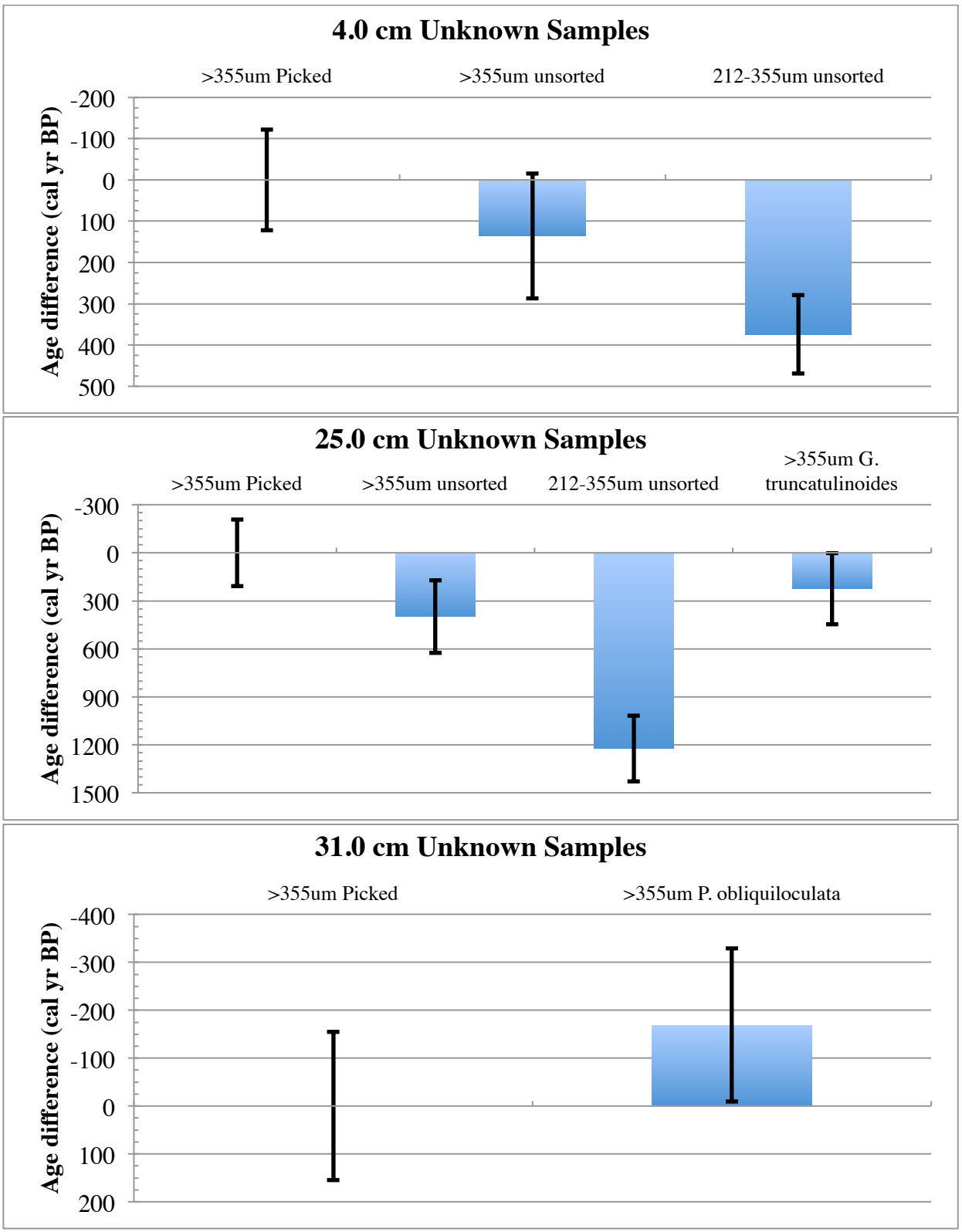

Figure 15: Age differences between the >355 μm picked sample and other chronometers of equivalent depth (4.0 cm, 25.0 cm and 31.0 cm) negative values are younger and positive values older.

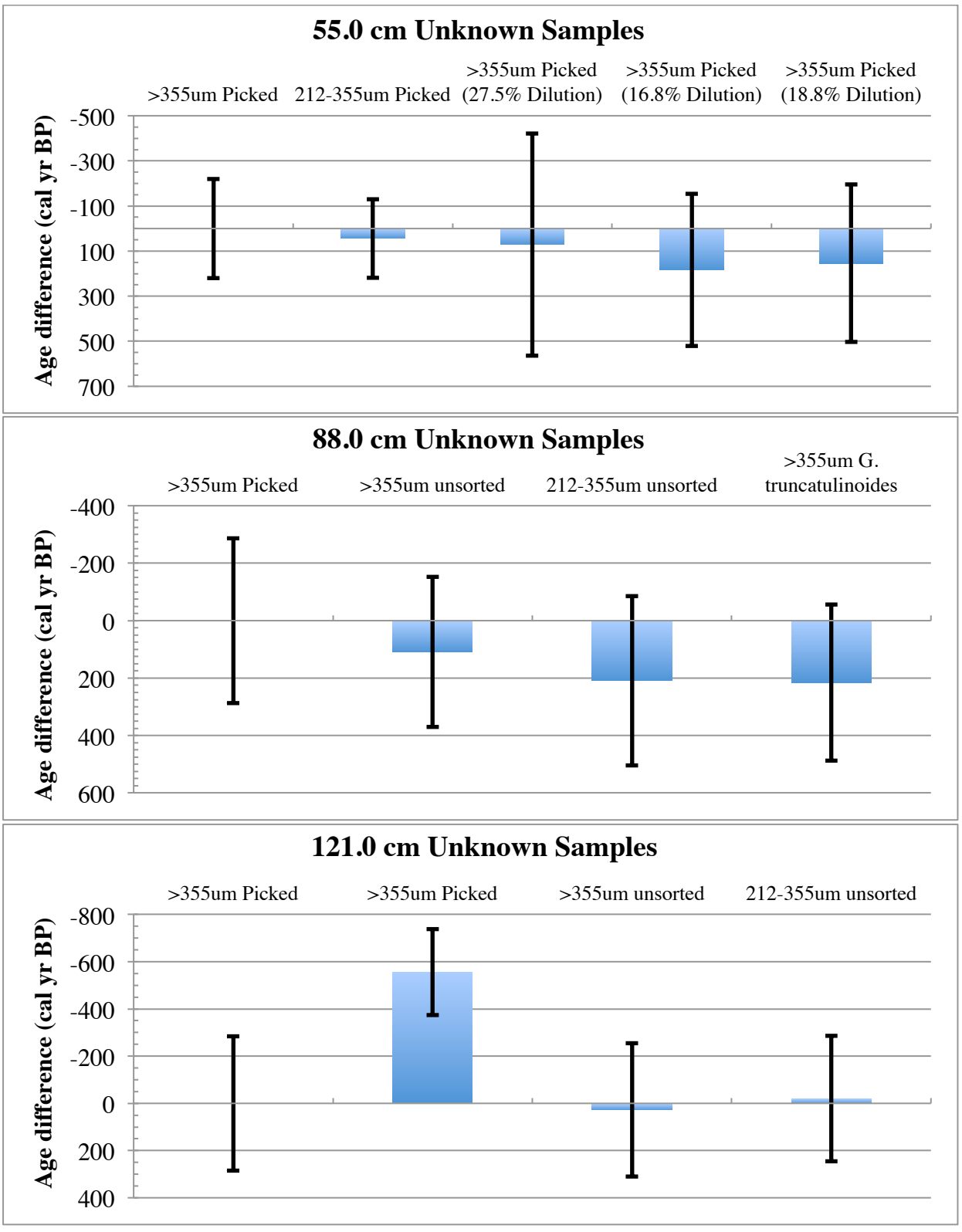

Figure 16: Age differences between the >355 μm picked sample and other chronometers of equivalent depth (55.0 cm, 88.0 cm and 121.0 cm) negative values are younger and positive values older.

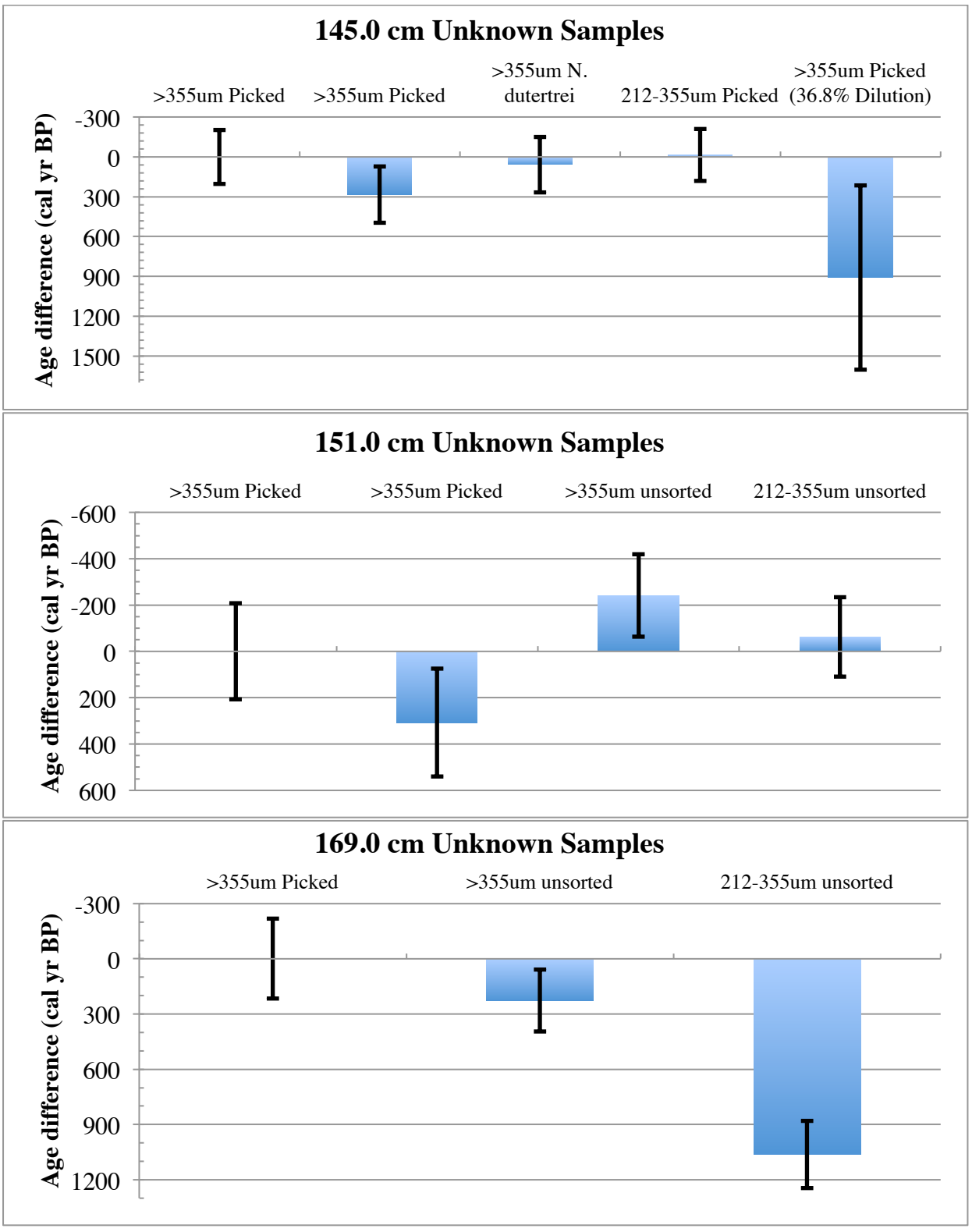

Figure 17: Age differences between the >355 µm picked sample and other chronometers of equivalent depth (145.0 cm, 151.0 cm and 169.0 cm) negative values are younger and positive values older.

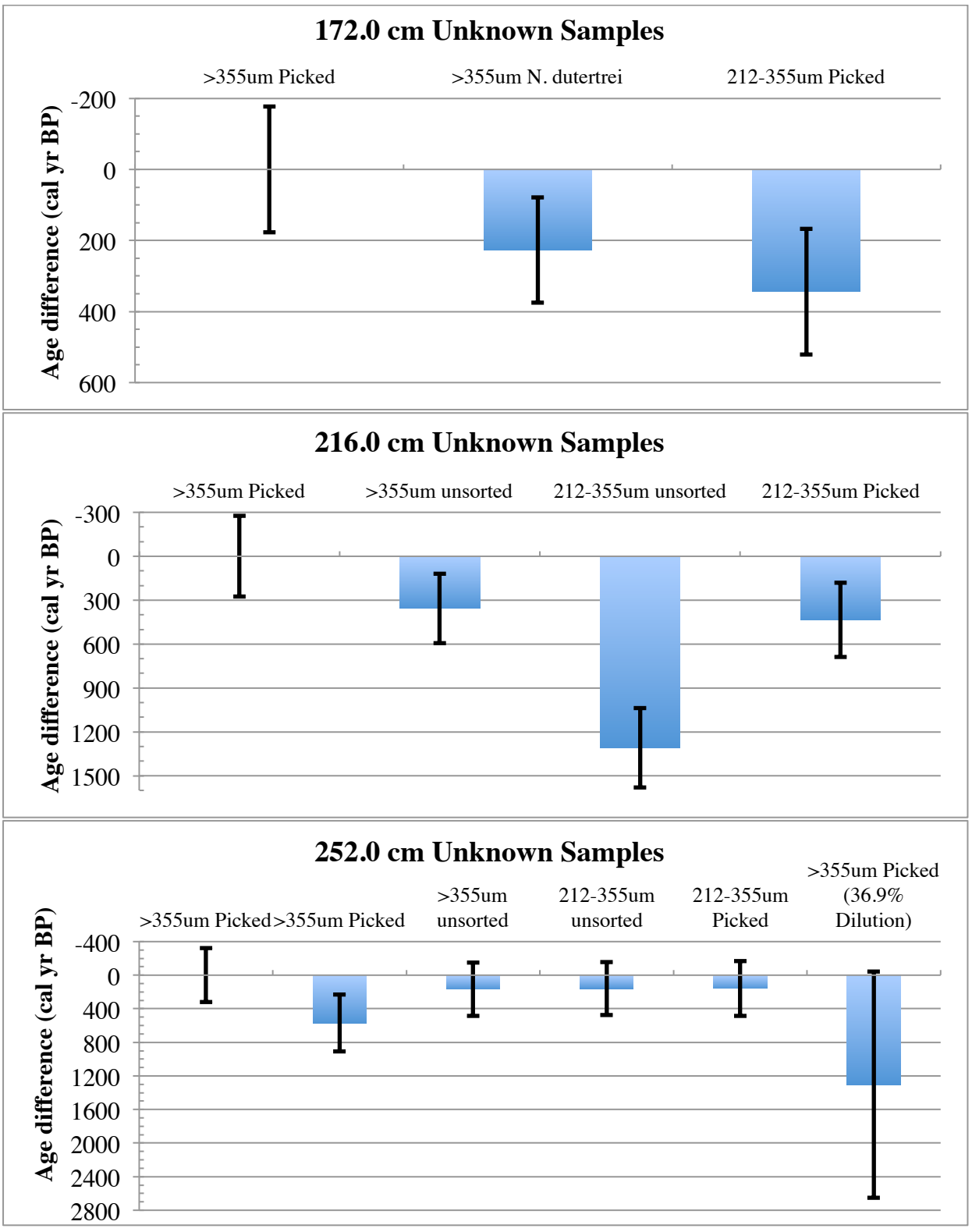

Figure 18: Age differences between the >355 µm picked sample and other chronometers of equivalent depth (172.0 cm, 216.0 cm and 252.0 cm) negative values are younger and positive values older.

3.2.2 Stable isotope results

Data from two *T. sacculifer* samples were rejected due to N_2 background recorded by the instrument, indicating a leak allowed atmospheric air into the system. *T. sacculifer* resides in the water column above the thermocline. $\delta^{13}C$ ranged from 2.052-2.747‰ (Figure 19) with a standard deviation of 0.19‰. *G. menardii* resides in the water column at or below the thermocline, and displayed a highly variable $\delta^{13}C$ at the modern part of the archive. At approximately 3450 cal. yr B.P. a trend was present as $\delta^{13}C$ became more isotopically depleted with time. $\delta^{13}C$ ranges from 1.379-2.398‰ (Figure 19) with a standard deviation of 0.29‰.

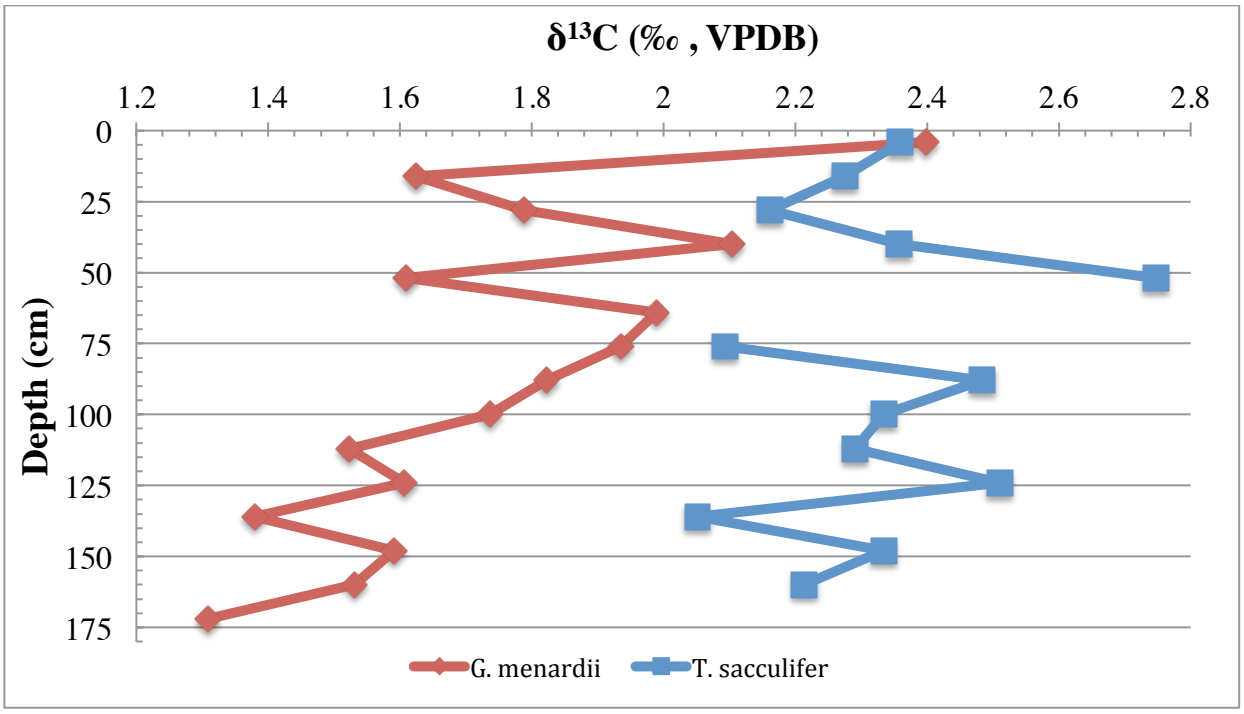

Figure 19. $\delta^{13}C$ for *T. sacculifer* (blue) and *G. menardii* (red) from Core PE-13-33-7 GC-5

The $\delta^{18}O$ relationship between *T. sacculifer* and *G. menardii* illustrates that these species reside at different depths in the water column (Ravelo and Hillaire-Marcel, 2007). *T. sacculifer* $\delta^{18}O$ ranged from -1.312 to -0.57‰ (Figure 20) with a standard deviation of 0.23‰. *G. menardii* $\delta^{18}O$ ranged from -0.256-0.759‰ (Figure 20) with a standard deviation of 0.28‰.

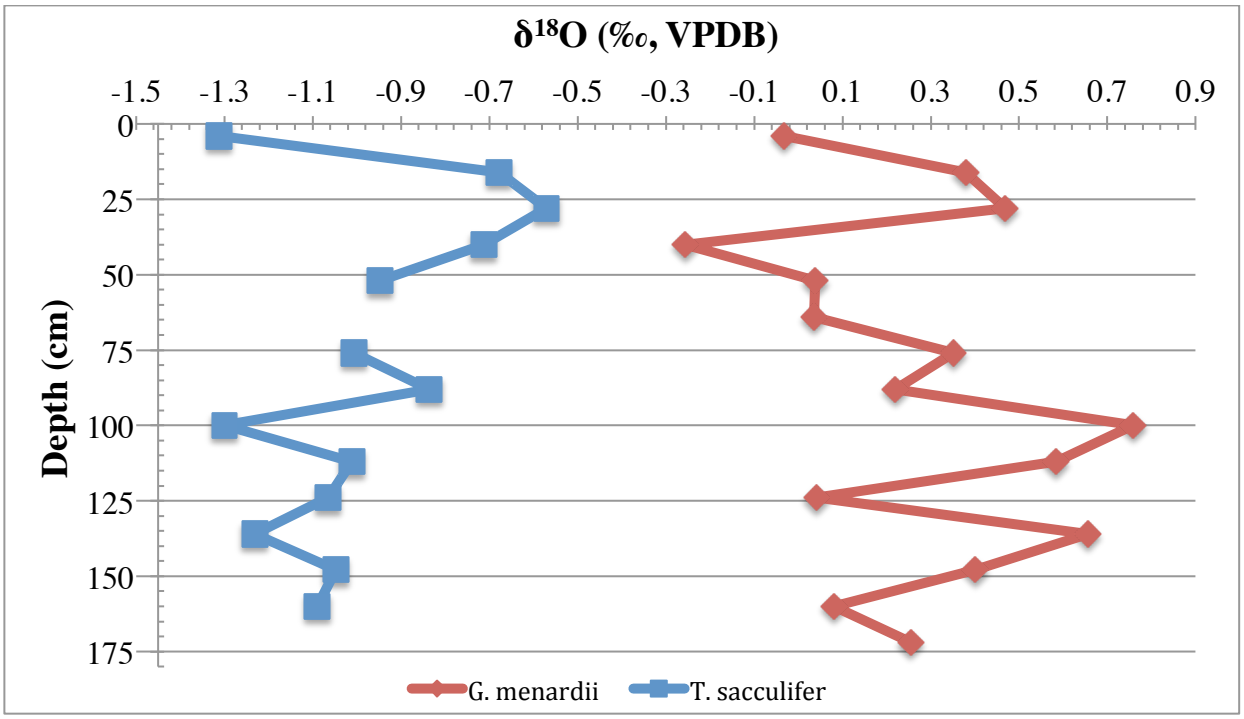

Figure 20. $\delta^{18}O$ for *T. sacculifer* (blue) and *G. menardii* (red) from Core PE-13-33-7 GC-5

3.3 Supplementary discussion

3.3.1 Chronology comparison

The overarching purpose of this research was to assemble a chronology for PE13-33-7 GC-5 using GIS-AMS ^{14}C measurements, however several other pertinent experiments were investigated to understand the age variance of different material types deposited at identical depths. The age fluctuation between samples from equivalent depths was likely due to a combination of redeposition, dissolution, recalcification, and diagenesis. Radiocarbon measurements of unsorted intervals, conceivably containing more fragmented, encrusted, imperfect foraminifera and other benthic foraminifera, radiolarians or pteropods produce a considerably older average age compared to that of the hand-picked intervals. These results indicate that the tedious microscope work of separating ideal foraminifer tests was necessary to

avoid age bias. If a slumping event occurred or bottom turbidity currents were present, smaller 212-355 μm tests are more likely to be reworked, or travel further. This could help explain the older average age when compared to the >355 μm picked mixed planktics. Reducing the GIS-AMS requested 25 mg sample size would help preserve priority material for additional isotopic research, however the amplified error involved with the isotope dilution of small samples proves this dating method inadequate for chronological purposes.

The species-specific ^{14}C measurements suggested that the reservoir age associated with carbonates could change due to the depth carbonate is precipitated at (Stuiver and Braziunas, 1993; Flower et al., 2011). The younger age of the more robust *P. obliquiloculata* refutes the likelihood of reworking (Broecker et al., 2006). *P. obliquiloculata* and *N. dutertrei* are abundant below the seasonal thermocline at about 50-70 m and 50-150 m water depth, where *G. truncatulinoides* begins life in equivalent shallow depths but adults may continue to calcify deeper in the water column about 200-250 m (Ravelo and Fairbanks 1992; Farmer et al., 2007; Spear et al., 2011). The species of planktic foraminifera selected for this research derived calcite from the DIC pool located in the mixed layer above the thermocline. Assemblage differences between depth intervals could have induced a small age variation depending on the ratio of deep to shallow species and where they were harvesting the DIC used for calcification. Foraminifera exhibit varying morphologies, thus experience differential settling through the water column; this induced minuscule age error when compared to the possible redeposition, dissolution or diagenesis of the planktic foraminifera test (Berger and Piper 1972, Wycech et al., 2016).

An objective of this research was to compare the novel chronological method using a Bayesian statistical accumulation program to guide ^{14}C measurements with traditional avenue of chronologies generated by the more analytically precise cesium sputter source. Box core MD02-

2553 was an excellent candidate for comparison, previously collected less than three kilometers from the location of gravity core PE13-33-7 GC-5. MD02-2553 experienced an overall faster accumulation rate likely due to a concentrated sedimentation effect towards the middle of the basin. The resolution of the PE13-33-7 GC-5 chronology was much poorer with few dates compared to the MD02-2553 chronology. As more dates were incorporated into the chronologies and funding exhausted, the PE13-33-7 GC-5 had a 95% confidence range 100 years more constrained than MD02-2553 (Figures 21-23). The age uncertainty of PE13-33-7 GC-5 seemed to approach an asymptote, probably due to a mixture of error from the instrument as well as the Bacon calibration.

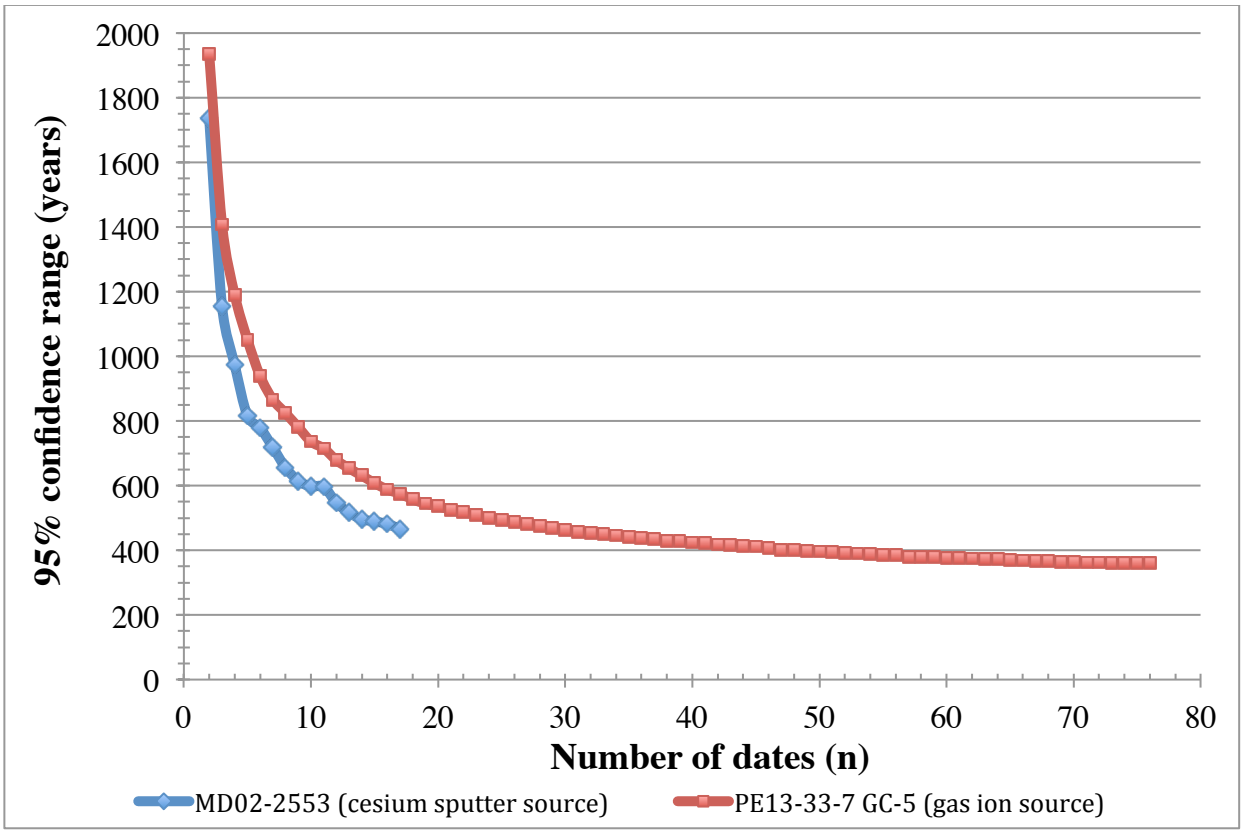

Figure 21: PE13-33-7 GC-5 and MD02-2553 equivalent analytical cost chronology comparison.

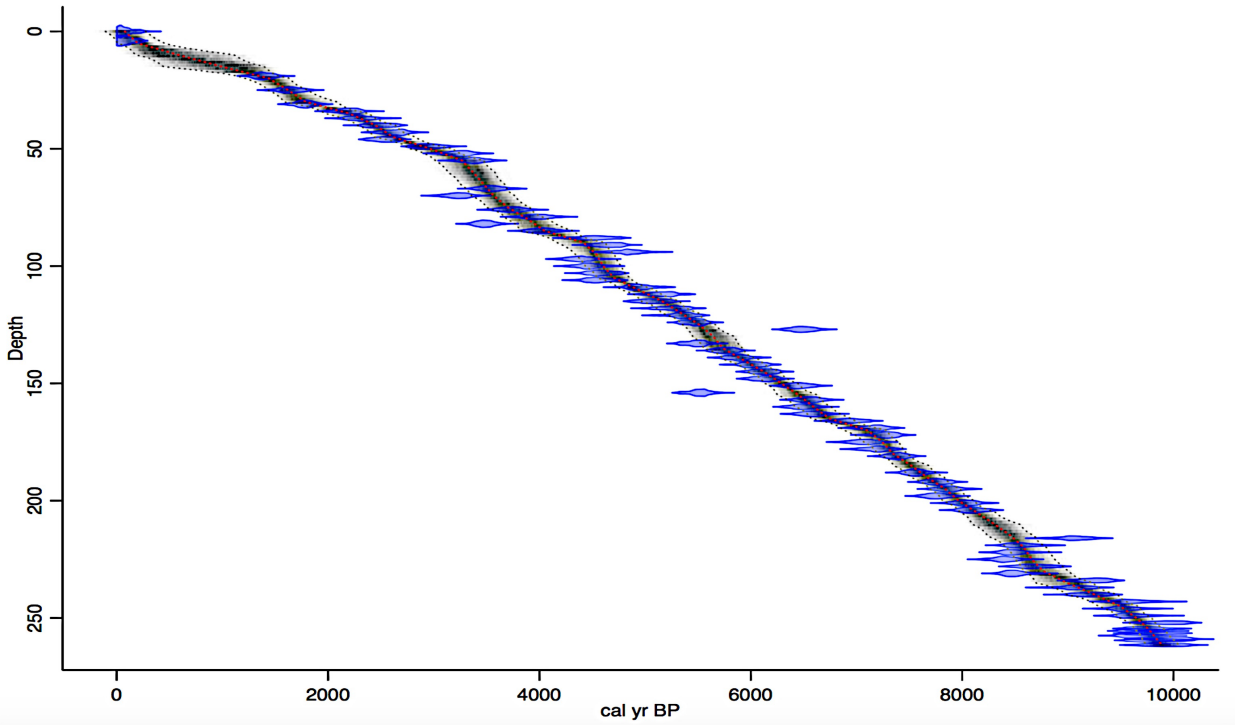

Figure 22: Bacon chronology using 75 Gas Ion Source dates for core PE13-33-7 GC-5

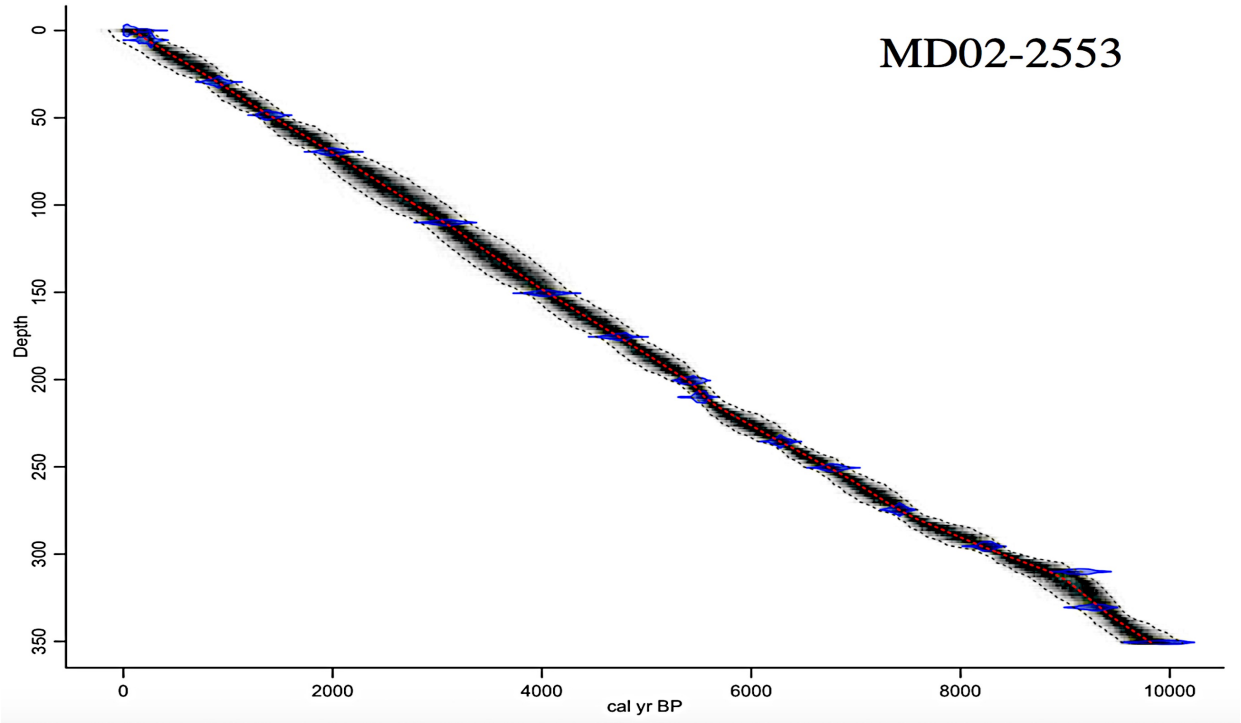

Figure 23: Bacon chronology using 16 cesium sputter source dates for core MD02-2553 (Poore et al., 2004).

This approach offers scientists the ability to quickly construct a strong chronology for an archive, while also permitting them to hone in on specific areas of interest where higher precision dating is required. Some scientific questions revolve around determining the exact date of historical events for example such as human migrations, the eruption of a volcano, or an extraterrestrial impact. More often it is necessary to accurately and precisely date hiatuses, changes in lithology, and instantaneous deposits such as slump events or turbidites. PE13-33-7 GC-5 displays stable sedimentation and contains only one hiatus interval. An additional strength of this chronological method is the possibility to combine multiple forms of dating including conventional graphitization AMS ^{14}C dates to improve precision in particular depths of the archive, thereby developing a chronology to the specific needs of the scientific question posed. The GC-5 chronology built with high-throughput dating was quite strong, however when fused with conventional graphitization ^{14}C dates the minimum and maximum uncertainty ages of the archive significantly decreased (Figure 6A).

3.3.2 Stable isotope interpretation

Planktic foraminifera tests provide Holocene records of past conditions in the water column above Pigmy basin. Stable isotope analyses for *Trilobatus sacculifer* and *Globorotalia menardii* were conducted to establish isotopic signatures of water masses above and at the thermocline. These data coupled with ^{14}C ages from PE-13-33-7 GC-5 show the evolution of $\delta^{13}C$ and $\delta^{18}O$ over geologic time. Stable isotope measurements were comparable to previous work in the Pigmy and Orca Basins (Kennett et al., 1985; Flower and Kennett, 1990; Flower et al., 2004; Richey et al., 2007; Montero-Serrano et al., 2010).

Isotopically light $\delta^{13}C$ signals recorded in foraminifera may indicate the strengthening of Mississippi river discharge, incorporating allochthonous carbon and likely causing skewing the

^{14}C reservoir age to an older value. A study by Lane et al., 2007 found that Mississippi estuarine chlorophyll a concentrations decreased when riverine output increased, due to reduced residence time of the water mass, and escalated turbidity (Lane et al., 2007). The Mississippi output was isotopically light ($\delta^{13}C$: -11‰ to -5‰) compared to marine values closer to 0-1‰, periods of substantial riverine flux potentially recorded as a signal in the tests of planktic foraminifera (Grossman and Ku, 1986; Brown and Kennett, 1999). Strong fluxes conceivably introduce a higher percentage of older allochthonous carbon with the autochthonous carbon found in the water column. Reservoir age of carbonates can change due to the sources of carbon present and the depth carbonate is precipitated. The variation of $\delta^{13}C$ between shallow and deep-water foraminifera species deposited contemporaneously could be used as a proxy for the fluctuation of reservoir age.

The $\delta^{13}C$ data follow the typical isotopic composition of the water column. *T. sacculifer* displays high deviation, but a large component of this fluctuation can be attributed to the intra-species vital effects of the individuals analyzed and should not be attributed to the variation in Mississippi river discharge. While *G. menardii* does become isotopically depleted, this deeper dwelling species resides at or below the thermocline, likely avoiding freshwater Mississippi discharge completely. It was interesting that *T. sacculifer* displayed a higher standard deviation than *G. menardii*, potentially explained by more variable thermocline water composition.

The ^{18}O to ^{16}O ratio of foraminifera is influenced by three parameters: the salinity and temperature of the water mass from which these organisms calcify from as well as the volume of ice on Earth. $\delta^{18}O$ records are difficult to analyze because the fluctuating sea surface temperatures and oxygen isotopic composition of seawater. Future research could utilize prior coral data to correct for ice volume and supplemental Mg/Ca measurements to interpret the

temperature of the water these foraminifera inhabited. Knowledge of $\delta^{18}O$ and Mg/Ca data allows for the calculation of temperature and salinity of surface waters throughout time. The $\delta^{18}O$ data suggested that these two species resided at different depths in the water column. The $\delta^{18}O$ record of *T. sacculifer* followed that of *G. menardii* closely from 0-40 cm however these records diverged after 40 cm, encountering maximum and minimum values at alternating depths. Additional isotopic analyses to provide more concentrated data would help improve the resolution of this study.

A core in closer proximity to the Mississippi river mouth with a high sedimentation rate and exceptional chronology is needed to test the hypothesis: $\delta^{13}C$ signatures from shallow and deep-water foraminifera deposited contemporaneously can be used as a proxy for the evolution of reservoir age over time.

3.4 Conclusions

- Coupling a Bayesian statistical accumulation model to instruct Gas-Ion Source measurements offers the ability to help resolve the timing of paleoenvironmental events by helping build more comprehensive age models in areas where an abundance of dateable material is present. This approach required less interpolation between discrete data points and resulted in better chronostratigraphic characterization of the archive when compared to a previously established chronology.
- The application of the Bayesian statistical accumulation model and Gas-Ion Source in tandem guided real-time ^{14}C measurements by identifying each subsequent interval to quantify. Non-sequential dating iteratively improved uncertainty but with diminishing return on age constraint, providing the operator with knowledge on when to conclude analysis.

- This method can be used in combination with conventional graphitization ^{14}C dates, as provision of denser dating around a precise baseline chronology. Additionally conventional AMS dates with higher precision can be used to improve a Bayesian model that shows a higher frequency of reversals, hiatuses, etc. than occurred in this core.
- These data buck a decades-long trend of advancing the physics and chemistry of dating, exclusively focused on improving measurement precision. The results of this study promote a shift from quality to quantity of measurements, with focus on reducing and improving the interpolation associated with age modeling of geologic archives.

List of References

Alvarez, L.W., and Cornog, R., 1939, Helium and Hydrogen of Mass 3: Physical Review, v. 56, no. 379, p. 613.

Anderson, E.C., Libby, W.F., Weinhouse, S., Reid, A.F., Kirshenbaum, A.D., and Grosse, A.V., 1947, Natural Radiocarbon from Cosmic Radiation: Science, v. 105, no. 2735, p. 576-577, doi:10.1126/science.105.2735.576.

Ascough, P.L., Cook, G.T., Church, M.J., Dugmore, A.J., McGovern, T.H., Dunbar, E., Einarsson, A., Friðriksson, A., and Gestsdóttir, H., 2009, Reservoirs and radiocarbon: ^{14}C dating problems in Myvatnssveit, Northern Iceland: Radiocarbon, v. 49, p. 947-961.

Bard, E., Arnold, M., Hamelin, B., Tisnerat-Laborde, N., and Cabioch, G., 1998, Radiocarbon calibration by means of mass spectrometric $^{230}Th/^{234}U$ and ^{14}C ages of corals: An updates database including samples from Barbados, Mururoa and Tahiti: Radiocarbon, v. 40, no. 3, p. 1085-1092.

Beaupré S.R., Roberts, M.L., Burton, J.R., and Summons, R.E., 2015, Rapid, high-resolution ^{14}C chronology of ooids: Geochemica et Cosmochimica Acta, v. 159, p. 126-138,

Behre, K.E., and van der Plicht, J., 1992, Towards an absolute chronology for the last glacial period in Europe: Radiocarbon dates from Oerel, northern Germany: Vegetation History and Archaeobotany, v. 1, no. 2, p. 111-117.

Bennett, C.L., Beukens, R.P., Clover, M.R., Gove, H.E., Liebert, R.B., Litherland, A.E., Purser, K.H., and Sondheim, W.E., 1977, Radiocarbon dating using electrostatic accelerators: negative ions provide the key: Science, v. 198, no. 4316, p. 508-510.

Berger, W.H., and Piper, D.J.W., 1972, Planktonic foraminifera: Differential settling, dissolution and redeposition: Limnology and Oceanography, v. 17, no. 2, p. 275-287, doi:10.4319/lo.1972.17.2.0275.

Berger, W.H., Killingley, J.S., and Vincent, E., 1978, Stable isotopes in deep-sea carbonates: Box core ERDC-92, west equatorial Pacific: Oceanologica Acta, v. 1, no. 2, p. 203-216.

Bird, M.I., Firfield, L.K., Santos, G.M., Beaumont, P.B., Zhou, Y., di Tada, M.L., and Hausladen, P.A., 2003, Radiocarbon dating from 40 to 60 ka BP at Border Cave, South Africa: Quaternary Science Reviews, v. 22, no. 8, p. 943-947, doi:10.1016/S0277-3791(03)00005-2.

Blaauw, M., 2010, Out of tune: the dangers of aligning proxy archives: Quaternary Science Reviews, v. 30, p. 1-12.

Blaauw, M., and Christen, J.A., 2011, Flexible paleoclimate age-depth models using an autoregressive gamma process: Bayesian Analysis, v. 6, no. 3, p. 457-474.

Broecker, W.S., Matsumoto, K., and Clark, E., 1999, Radiocarbon age differences between coexisting foraminiferal species: Paleoceanography, v. 14, no. 4, p. 431-436.

Broecker, W.S., Barker, S., Clark, E., Hajdas, I., and Bonani, G., 2006, Anomalous radiocarbon ages for foaminifera shells: Paleoceanography, v. 21, no. 2, doi:10.1029/2005PA001212.

Brown, P., and Kennett, J.P., 1999, Marine evidence for episodic Holocene megafloods in North America and the northern Gulf of Mexico: Paleoceanography, v. 14, no. 4, p. 498-510, doi:10.1029/1999PA900017.

Buck, C.E., Kenworthy, J.B., Litton, C.D., and Smith, A.F.M., 1991, Combining archaeological and radiocarbon information: a Bayesian approach to calibration: Antiquity, v. 65, p. 808-821.

Burke, A., Robinson, L.F., McNichol, A.P., Jenkins, W.J., Scanlon, K.M., and Gerlach, D.S., 2010, Reconnaissance dating: A new radiocarbon method applied to assessing the temporal distribution of Southern Ocean deep-sea corals: Deep-Sea Research I, v. 57, no. 11, p. 1510-1520, doi:10.1016/j.dsr.2010.07.010.

Burman, J., Gustafsson, O., Segl, M., and Schmitz, B., 2005, A simplified method of preparing phosphoric acid for stable isotope analyses of carbonates: Rapid Communications Mass Spectrometry, v. 19, p. 3086–3088, doi:10.1002/rcm.2159.

Burr, G.S., Beck, J.W., Taylor, F.W., Récy, J., Edwards, R.L., Cabioch, G., Corrège, T., Donahue, D.J., and O'Malley J.M., 1998, A high-resolution radiocarbon calibration between 11,700 and 12,400 calendar years BP derived from ^{230}Th ages of corals from Espiritu Santo Island, Vanuatu: Radiocarbon, v. 40, no. 3, p. 1093-1105.

Christen, J.A., 1994, Bayesian interpretation of radiocarbon results: University of Nottingham, Thesis.

Christen, J.A., 1994, Summarizing a set of radiocarbon determinations – a robust approach: Applied Statistics, v.43, p. 489-503.

Christen, J.A., and Pérez, E., 2009, A new robust statistical model for radiocarbon data: Radiocarbon, v. 51, no. 3, p. 1047-1059.

Coplen, T.B., 2011, Guidelines and recommended terms for expression of stable-isotope-ratio and gas-ratio measurements results: Rapid Communications in Mass Spectrometry, v. 25, p. 2538-2560, doi:10.1002/rcm.5129.

Coplen, T.B., Brand, W.A., Gehre, M., Gröning, M., Meijer, H.A.J., Toman, B., and Verkouteren, R.M., 2006, New guidelines for $\delta^{13}C$ measurements: Analytical Chemistry, v. 78, no. 7, p. 2439-2441, doi:101.1021/ac052027c.

De Rooij, M., van der Plicht, J., and Meijer, H.A.J., 2008, Sample dilution for AMS ^{14}C analysis of small samples (30-150ug C): Radiocarbon, v. 50, no. 3, p. 413-436.

De Vleeschouwer, D., and Parnell, A. C., 2014, Reducing time-scale uncertainty for the Devonian by integrating astrochronology and Bayesian statistics: Geology, v. 42, p. 491-494.

de Vries, H., 1958, Variations in concentration of radiocarbon with time and location on Earth: Akademie Van Wet.

Druffle, E.R.M., and Williams, P.M., 1991, Radiocarbon in seawater and organisms from the Pacific coast of Baja California: Radiocarbon, v. 33, no. 3, p. 291-296.

Duhr, A., and Hilkert, A.W., 2004, δ18O and δ13C Determination of Carbonates Using Thermo Scientific GasBench II. Thermo Fisher Scientific Application Note 30050.

Edwards, R.L., Beck, J.W., Burr, G.S., Donahue, D.J., Chappell, J.M.A, Bloom, A.L., Druffel, E.R.M., and Taylor, F.W., 1993, A large drop in atmospheric $^{14}C/^{12}C$ and reduced melting in the Younger Dryas, documented with ^{230}Th ages of corals: Science, v. 260, p. 962-968.

Egan, J., Staff, R., and Blackford, J., 2015, A revised age estimate of the Holocene Plinian eruption of Mount Mazama, Oregon using Bayesian statistical modeling: The Holocene, v. 27, p. 1054-1067, doi:10.1177/0959683615576230.

Elderfield, H., Vautraver, M., and Cooper, M., 2002, The relationship between shell size and Mg/Ca, Sr/Ca, $\delta^{18}O$, and $\delta^{13}C$ of species of planktonic foraminifera: Geochemistry, Geophysics, Geosystems, v. 3, n. 8, p. 1-13, doi:10.1029/2001GC000194.

Enkin, R.J., Dallimore, A., Baker, J., Southon, J.R., and Ivanochko, T., 2013, A new high-resolution radiocarbon Bayesian age model of the Holocene and Late Pleistocene from core MD02-2494 and others, Effingham Inlet, British Columbia, Canada; with an application to the paleoseismic event chronology of the Cascadia Subduction Zone: Canada Journal of Earth Sciences, v. 50, no. 7, p. 746-760.

Farmer, E.C., Kaplan, A., de Menocal, P.B., and Lynch-Stieglitz, J., 2007, Corroborating ecological depth preferences of planktonic foraminifera in the tropical Atlantic with the stable oxygen isotope ratios of core top specimens: Paleoceanography, v. 22, no. 3, doi:10.1029/2006PA001361.

Flower, B.P., Hastings, D.W., and Randle, N.J., 2011, Paired AMS ^{14}C dates on planktic foraminifera from a Gulf of Mexico sediment core: an assessment of stratigraphic continuity: Radiocarbon, v. 53, p. 337-344.

Flower, B.P., Hastings, D.W., Hill, H.W., and Quinn, T.M., 2004, Phasing of deglacial warming and Laurentide Ice Sheet meltwater in the Gulf of Mexico: Geology, v. 32, no. 7, p. 597-600, doi:10.1130/G20604.1.

Flower, B. P., and Kennett, J.P., 1990, The Younger Dryas cool episode in the Gulf of Mexico: Paleoceanography, v. 5, no. 6, p. 949-961.

Gillespie, R., Polach, H.A., and Temple, R.B., 1972, Sydney University Natural Radiocarbon Measurements I: Radiocarbon, v. 14, no. 2, p. 413-417.

Goodfriend, A.G., and Flessa, K.W., 1997, Radiocarbon reservoir ages in the Gulf of California: Roles of upwelling and flow from the Colorado River: Radiocarbon, v. 39, p. 139-148.

Grossman, E.L., and Ku, T., 1986, Oxygen and carbon isotope fractionation in biogenic aragonite: temperature effects: Chemical Geology, v. 59, p. 59-74.

Han, B.X., Von Reden, K.F., Roberts, M.L., Schneider, R.J., Hayes, J.M. and Jenkins, W.J., 2007, Electromagnetic field modeling and ion optics calculations for a continuous-flow AMS system: Nuclear Instruments and Methods in Physics Research, v. 259, no. 1, p. 111-117, doi:10.1016/j.nimb.2007.01.224.

Haslett, J., and Parnell, A., 2008, A simple monotone process with application to radiocarbon-dated depth chronologies: Journal of the Royal Statistical Society: Series C, v. 57, no. 4, p. 399-418.

Hughen, K.A., Baillie, M.G.L., Bard, E., Bayliss, A., Beck, J.W., Bertrand, C.J.H., Blackwell, P.G., Buck, C.E., Burr, G.S., Cutler, K.B., Damon, P.E., Edwards, R.L., Fairbanks, R.G., Friedrich, M., Guilderson, T.P., Kromer, B., McCormac, F.G., Manning, S.W., Bronk Ramsey, C., Reimer, P.J., Reimer, R.W., Remmele, S., Southon, J.R., Stuiver, M., Talamo, S., Taylor, F.W., van der Plicht,. J, Weyhenmeyer, C.E., 2004, a. Marine04 Marine radiocarbon age calibration, 26 - 0 ka BP: Radiocarbon, v. 46, no. 03, p. 1059-1086.

Jasper, J.P., and Gagosian, R.B., 1990, The sources and deposition of organic matter in the Late Quaternary Pigmy Basin, Gulf of Mexico: Geochimica et Cosmochimica Acta, v. 54, no. 4, p. 1117-1132, doi:10.1016/0016-7037(90)90443-O.

Jazwa, C.S., Gamble, L.H., and Kennett, D.J., 2013, A high-precision chronology for two house features at an early village site on western Santa Cruz Island, California, USA: Radiocarbon, v. 55, no. 01, p. 185-199.

Jones, K.B., Hodgins, G.W.L., Etayo-Cadavid, M.F., Andrus, C.F.T. and Sandweiss, D.H., 2010, Centuries of marine radiocarbon reservoir age variation within archaeological *mesodesma donacium* shells from southern Peru: Radiocarbon, v. 52, p. 1207-1214.

Kennett, D.J., Ingram, B.L., Erlandson, J.M., and Walker, P., 1997, Evidence for temporal fluctuations in marine radiocarbon reservoir ages in the Santa Barbara Channel, Southern California: Journal of Archeological Science, v. 24, p. 1051-1059.

Kennett, J.P., Elmstrom, K., and Penrose, N., 1985, The last deglaciation in Orca Basin, Gulf of Mexico—high resolution planktonic foraminiferal changes: Palaeogeography, Palaeoclimatology and Palaeoecology, v. 50, p. 189-216.

Klein, J., Lerman, J.C., Damon, P.E., and Ralph, E.K., 1982, Calibration of radiocarbon dates: Tables based on the consensus data of the workshop on calibrating the radiocarbon time scale: Radiocarbon, v. 24, no. 2, p. 103-150.

Kosnik, M.A., Hua, Q., Kaufman, D.S., and Zawaszki, A., 2015, Sediment accumulation, stratigraphic order, and the extent of time-averaging in lagoonal sediments: a comparison of ^{210}Pb and ^{14}C/amino acid racemization chronologies: Coral Reefs, v. 34, no. 1 p. 215-229, doi:10.1007/s00338-014-1234-2.

Lane, R.R., Day, J.W., Marx, B.D., Reyes, E., Hyfield, E., and Day, J.N., 2007, The effects of riverine discharge on temperature, salinity suspended sediment and chlorophyll a in a Mississippi delta estuary measured using a flow-through system: Estuarine, Coastal and Shelf Science, v. 74, no. 1, p. 145-154, doi:10.1016/j.ecss.2007.04.008.

Libby, W.F., 1967, History of radiocarbon dating: Symposium on Radiocarbon Dating and Methods of Low Level Counting, p. 3-26.

Libby, W.F., Anderson, E.C., and Arnold, J.R., 1949, Age determination by radiocarbon content: World-wide assay of natural radiocarbon: Science, v. 109, no. 2827, p. 227-228.

Longworth, B.E., Robinson, L.F., Roberts, M.L., Beaupre, S.R., Burke, A., and Jenkins W.J., 2013, Carbonate as sputter target material for rapid ^{14}C AMS: Nuclear instruments and Methods in Physics Research, v. 294, p. 328-334, doi:10.1016/j.nimb.2012.05.014.

Mangerud, J., 1972, Radiocarbon dating of marine shells, including a discussion of apparent age of recent shells from Norway: Boreas, v. 1, no. 2, p. 143-172.

McIntyre, C.P., Roberts, M.L., Burton, J.R., McNichol, A.P., Burke, A., Robinson, L.F., von Reden, K.F., and Jenkins, W.J., 2011, Rapid radiocarbon (^{14}C) analysis of coral and carbonate samples using a continuous-flow accelerator mass spectrometry (CFAMS) system: Paleoceanography, v. 26, no. 4, doi:10.1029/2011PA002174.

Montero-Serrano, J.C., Bout-Roumazeilles, V., Sionneau, T., Tribovillard, N., Bory, A., Flower, B., Riboulleau, A., Martinez P., and Billy I., 2010 Changes in precipitation regimes over North America during the Holocene as recorded by mineralogy and geochemistry of Gulf of Mexico sediments: Global and Planetary Change, v. 74, no. 3, p. 132-143, doi:10.1016/j.gloplacha.2010.09.004.

Montero-Serrano, J.C., Bout-Roumazeilles, V., Tribovillard, N., Sionneau, T., Riboulleau, A., Bory, A., and Flower, B., 2009, Sedimentary evidence of deglacial megafloods in the northern Gulf of Mexico (Pigmy Basin): Quaternary Science Reviews, v. 28, no. 27, p. 3333-3347, doi:10.1016/j.quascirev.2009.09.011.

Muller, R.A., 1977, Radioisotope Dating with a Cyclotron: Science, v. 196, no. 4289, p. 489-494.

Nelson, D.E., Korteling, R.G., and Scott, W.R., 1977, Carbon-14: direct-detection at Natural Concentrations: Science, v. 198, no. 4316, p. 507-508.

Nielsen, J., Hedeholm, R.B., Heinemeier, J., Bushnell, P.G., Christiansen, J.S., Olsen, J., Ramsey, C.B., Brill, R.W., Simon, M., Steffensen, K.F., and Steffensen J.F., 2016, Eye lens radiocarbon reveals centuries of longevity in the Greenland shark (*Somniosus microcephalus)*: Science, v. 353, p. 702-704.

Pearson, A., McNichol, A.P., Schneirder, R.J., Von Reden, K.F., and Zheng, Y., 1998, Microscale AMS ^{14}C measurement at NOSAMS: Radiocarbon, v. 40, no. 1, p. 61-75.

Polach, H.A., 1969, Optimisation of liquid scintillation radiocarbon age determinations and reporting of ages: Atomic Energy in Australia, v. 12, no. 3, p. 21-28.

Polach, H.A., 1987, Evaluation and status of liquid scintillation counting for radiocarbon dating: Radiocarbon, v. 29, no. 1, p. 1-11.

Polach, H.A., Gower, J., and Frazer, I., 1972, Synthesis of high purity benzene for radiocarbon dating by the liquid scintillation method, in Rafter, TA and Grant-Taylor, T, eds, International conference on radiocarbon dating, 8th, proceedings: Wellington, New Zealand, v. 1, p. 145-157.

Poore, R.Z., Dowsett, J.J., and Verardo, S., 2003, Millennial to century-scale variability in Gulf of Mexico Holocene climate records: Paleoceanography, v. 18, no. 2, p. 1048, doi:10.1029/2002PA000868.

Poore, R.Z., Quinn, T.M., and Verardo, S., 2004, Century-scale movement of the Atlantic Intertropical Convergence Zone linked to solar variability: Geophysical Research Letters, v. 31, no. 12, doi:10.1029/2004GL019940.

Poore, R.Z., Verardo, S., Caplan, J., Pavich, K., and Quinn, T., 2011, Planktic foraminiferal relative abundance trends in the Gulf of Mexico Holocene sediments: Records of climate variability, in Gulf of Mexico, Its Origins, Waters, Biota, and Human Impacts, v. 3, p. 367-379.

Ramsey, C.B., 1994, Analysis of chronological information and radiocarbon calibration: the program OxCal: Archaeological Computing Newsletter, v. 41, no. 11, p. e16.

Ramsey, C.B., 2009, Bayesian Analysis of Radiocarbon Dates: Radiocarbon, v. 51, p. 337-360.

Ramsey, C.B., 2009, Dealing with outliers and offsets in Radiocarbon dating: Radiocarbon, v. 51, no. 3, p. 1023-1045.

Ravelo, A.C., and Fairbanks, N.R.G., 1992, Oxygen isotope composition of multiple species of planktonic foraminifera: Recorders of the modern photic zone temperature gradient: Paleoceanography, v. 7, no. 6, p. 815-831, doi:10.1029/92PA02092.

Ravelo, A.C., and Hillaire-Marcel, C., 2007, The use of oxygen and carbon isotopes of foraminifera in paleoceanography: Developments in Marine Geology, chapter eighteen, v.1, p. 735-764, doi:10.1016/S1572-5480(07)01023-8.

Reimer, P.J., Baillie, M.G.L., Bard, E., Bayliss, A., Beck, J.W., Bertrand C.J.H., Blackwell, P.G., Buck, C.E., Burr, G.S., Cutler, K.B., Damon, P.E., Edwards, R.L., Fairbanks, R.G., Friedrich, M., Guilderson, T.P., Hogg, A.G., Hughen, K.A., Kromer, B., McCormac, G., Manning, S., Ramsey, C.B., Reimer, R.W., Remmele, S., Southon, J.R., Stuiver, M., Talamo, S., Tayler, F.W., van der Plicht, J., and Weyhenmeyer, C.E., 2004, INTCAL04 terrestrial radiocarbon age calibration, 0-26 cal kyr BP: Radiocarbon, v. 46, no. 3, p. 1029-1058.

Raymond, P.A., Oh, N., Turner, R.E., and Broussard, W., 2008, Anthropogenically enhanced fluxes of water and carbon from the Mississippi River: Nature, v. 451, p. 449-452, doi:10.1038/nature06505.

Révész, K.M., and Landwehr, J.M., 2002, δ13C and δ18O isotopic composition of CaCO3 measured by continuous flow isotope ratio mass spectrometry: statistical evaluation and verification by application to Devils Hole core DH-11 calcite: Rapid Communications Mass Spectrometry, v. 16, p. 2102–2114. doi:10.1002/rcm.833.

Richey, J.N., Hollander, D.J., Flower, B.P., and Eglinton, T.I., 2011, Merging late Holocene molecular organic and foraminiferal-based geochemical records of sea surface temperature in the Gulf of Mexico: Paleoceanography, v. 26, no. 1, doi:10.1029/2010PA002000.

Richey, J.N., Poore, R.Z., Flower, B.P., and Hollander, D.J., 2012, Ecological controls on the shell geochemistry of pink and white *Globigerinoides ruber* in the northern Gulf of Mexico: Implications for paleoceanographic reconstruction: Marine Micropalenontology, v. 82, p. 28-37.

Richey, J.N., Poore, R.Z., Flower, B.P., and Quinn, T.M., 2007, 1400 yr multiproxy record of climate variability from the northern Gulf of Mexico: Geology, v. 35, no. 5, p. 423-426, doi:10.1130/G23507A.1.

Ring, J.C., Nguyen, D.C., and Everett, L.J., 1980, Liquid scintillation counting from gross counts to spectral analysis, in Peng, C-T., Horrocks, D.L., and Alpen, E.L., Liquid scintillation counting, recent application and development: New York, Academic Press, v. 1, p. 89-104.

Roberts, M.L., Beaupré, S.R., and Burton, J.R., 2013, A high-throughput, low-cost method for analysis of carbonate samples for ^{14}C: Radiocarbon, v. 55, no. 2-3, p. 585-592.

Roberts, M.L., Von Reden, K.F., Burton, J.R., McIntyre, C.P., and Beaupré, S.R., 2013, A gas-accepting ion source for Accelerator Mass Spectrometry: Progress and applications: Nuclear instruments and Methods in Physics Research, v. 294, p. 296-299.

Rosenheim, B.E., Day, M.B., Domack, E., Schrum, H., Benthien, A., and Hayes, J.M., 2008, Antarctic sediment chronology by programmed-temperature pyrolysis: Methodology and data treatment: Geochemistry, Geophysics, Geosystems, v. 9, no. 4, doi:1029/2007GC001816.

Ruff, M., Wacker, L., Gäggeler, H.W., Suter, M., Synal, H-A., and Szidat, S., 2007, A gas ion source for radiocarbon measurements at 200kV: Radiocarbon, v. 49, no. 2, p. 307-314.

Ryan, W.B.F., Carbotte, S.M., Coplan, J.O., O'Hara, S., Melkonian, A., Arko, R., Weissel, R.A., Ferrini, V., Goodwillie, A., Nitsche, F., Bonczkowski, J., and Zemsky, R., 2009, Global Multi-Resolution Topography synthesis: Geochemistry, Geophysics, Geosystems, v. 10, no. 3, doi:10.1029/2008GC002332.

Santos, G.M., Moore, R.B., Southon, J.R., Griffin, S., Hinger, E., and Zhang, D., 2007, AMS ^{14}C sample preparation at the KCCAMS/UCI facility: status report and performance of small samples: Radiocarbon, v. 49, no. 2, p. 255-269.

Santos, G.M., Southon, J.R., Drenzek, N.J., Ziolkowski, L.A., Druffel, E., Xu, X., Zhang, D., Trumbore, S., Eglinton, T.I., and Hughen, K.A., 2010, Blank assessment for ultra-small radiocarbon samples: chemical extraction and separation versus AMS: Radiocarbon, v. 52, no. 3, p. 1322-1335, doi:https://doi.org/10.1017/S0033822200046415.

Shah, S.R., and Pearson, A., 2007, Ultra-microscale (5-25 µg C) analysis of individual lipids by ^{14}C AMS: Assessment and correction or sample processing blanks: Radiocarbon, v. 49, no. 1, p. 69-82.

Shah Walter, S.R., Gagnon, A.R., Roberts, M.L., McNichol, A.P., Lardie Gaylord, M.C., Klein, E., 2015, Ultra-small graphitization reactors for ultra-microscale ^{14}C analysis at the national ocean science accelerator mass spectrometry (NOSAMS) facility: Radiocarbon, v. 57, n. 1, p. 109-122, doi:10.2458/azu_rc.57.18118.

Spear, J.W., Poore, R.Z. and Quinn, T.M., 2011, *Globorotalia truncatulinoides* (dextral) Mg/Ca as a proxy for Gulf of Mexico winter mixed-layer temperature: Evidence form a sediment trap in the northern Gulf of Mexico: Marine Micropaleontology, v. 80, no. 3, p. 53-61, doi:10.1016/j.marmicro.2011.05.001.

Spero, H.J., and Lea, D.W., 1993, Intraspecific stable isotope variability in the planktic foraminifera *Globigerinoides sacculifer*: Results from laboratory experiments: Marine Micropaleontology, v. 22, p. 221-234.

Spero, H.J., Lerche, I., and Williams, D.F., 1991, Opening the carbon isotope "vital effect" black box, 2, quantitative model for interpreting foraminiferal carbon isotope data: Paleoceanography, v. 6, no. 6, p. 639-655, doi:10.1029/91PA02022.

Spötl, C., and Vennemann, T.W., 2003 Continuous-flow isotope ratio mass spectrometric analysis of carbonate minerals: Rapid Communications Mass Spectrometry, v. 17, p. 1004–1006, doi:10.1002/rcm.1010.

Stuiver, M., 1982, A high-precision calibration of the AD radiocarbon time scale: Radiocarbon, v. 24, no. 1, p. 1-26.

Stuiver, M., and Braziunas, T.F., 1993, Modeling atmospheric ^{14}C influences and ^{14}C ages of marine samples to 10,000 BC: Radiocarbon, v. 35, no. 1, p. 137-189.

Stuiver, M., and Reimer, P.J., 1986, A computer program for radiocarbon age calibration: Radiocarbon, v. 28, no. 2B, p. 1022-1030.

Stuiver, M., Heusser, C.J., and Yang, I.C., 1978, North American glacial history extended to 75,000 years ago: Science, v. 200, no. 4337, p. 16-21.

Stuiver, M., Pearson, G.W., and Braziunas, T., 1986, Radiocarbon age calibration of marine samples back to 9000 cal. yr BP: Radiocarbon, v. 28, no. 2B, p. 980-1021.

Stuiver, M., Reimer, P.J., and Reimer, R.W., 2017, CALIB 7.1 [WWW program] at http://calib.org, accessed 2017-1-31.

Sveinbjörnsdóttir, Á.E., Ramsey, C.B., and Heinemeier, J., 2016, The settlement date of Iceland revisited: Evaluation of ^{14}C dates from sites of early settlers in Iceland by Bayesian statistics: Radiocarbon, v. 58, no. 2, p. 235-245, doi:10.1017/RDC.2016.2.

Synal, H-A., Stocker, M., and Suter, M., 2007, MICADAS: A new compact radiocarbon AMS system: Nuclear instruments and Methods in Physics Research, v. 259, no. 1, p. 7-13, doi:10.1016/j.nimb.2007.01.138.

Thiagarajan, N., Gerlach, D., Roberts, M.L., Burke, A., McNichol, A., Jenkins, W.J., Subhas, A.V., Thresher, R.E., and Adkins, J.F., 2013, Movement of deep-sea coral populations on climatic timescales: Paleoceanography, v. 28, no. 2, p. 227-236, doi:10.1002/palo.20023.

Von Reden, K.F., Roberts, M.L., Jenkins, W.J., Rosenheim, B.E., McNichol, A.P., and Schneider, R.J., 2008, Software development for continuous-gas-flow AMS: Nuclear instruments and Methods in Physics Research, v. 266, no. 10, p. 2233-2237.

Von Reden, K.F., Roberts, M.L., McIntyre, C.P., and Burton, J.R., 2011, Design and Reality: Continuous-flow Accelerator Mass Spectrometry (CFAMS): Nuclear instruments and Methods in Physics Research, v. 269, no. 24, p. 3176-3179.

Wycech, J., Kelly, D.C., and Marcott, S., 2016, Effects of seafloor diagenesis on planktic foraminiferal radiocarbon ages: Geology, v. 44, no. 7, p. 551-554, doi:10.1130/G37864.1.

Appendices

Appendix A: Grain size data

Sample Name	Depth (cm)	%Clay	%Silt	%Sand
PE 13-33-7 2-3cm - Average	2.5	29.33	61.86	8.81
PE 13-33-7 5-6cm - Average	5.5	30.87	66.74	2.40
PE 13-33-7 7.5-8.5cm - Average	8.0	31.67	64.59	3.73
PE 13-33-7 10-11cm - Average	10.5	30.93	64.36	4.71
PE 13-33-7 12-13cm - Average	12.5	30.98	65.66	3.35
PE 13-33-7 14-15cm - Average	14.5	31.56	64.10	4.34
PE 13-33-7 15-16cm - Average	15.5	34.56	64.05	1.39
PE 13-33-7 16-17cm - Average	16.5	33.24	63.53	3.22
PE 13-33-7 20-21cm - Average	20.5	63.37	35.26	1.37
PE 13-33-7 30-31cm - Average	30.5	66.77	30.82	2.41
PE 13-33-7 40-41cm - Average	40.5	32.81	65.04	2.15
PE 13-33-7 50-51cm - Average	50.5	31.74	64.93	3.33
PE 13-33-7 60-61cm - Average	60.5	36.47	63.16	0.37
PE 13-33-7 70-71cm - Average	70.5	29.99	67.83	2.19
PE 13-33-7 80-81cm - Average	80.5	31.59	62.47	5.95
PE 13-33-7 90-91cm - Average	90.5	60.94	37.45	1.61
PE 13-33-7 100-101cm - Average	100.5	34.31	60.30	5.39
PE 13-33-7 110-111cm - Average	110.5	27.93	58.97	13.10
PE 13-33-7 120-121cm - Average	120.5	31.27	62.64	6.09
PE 13-33-7 130-131cm - Average	130.5	35.91	61.99	2.10
PE 13-33-7 140-141cm - Average	140.5	31.85	63.89	4.26
PE 13-33-7 150-151cm - Average	150.5	31.24	58.79	9.97
PE 13-33-7 160-161cm - Average	160.5	32.41	60.84	6.76
PE 13-33-7 170-171cm - Average	170.5	37.37	60.51	2.12
PE 13-33-7 180-181cm - Average	180.5	35.12	63.22	1.66
PE 13-33-7 190-191cm - Average	190.5	34.90	61.17	3.93
PE 13-33-7 200-201cm - Average	200.5	36.41	60.41	3.18
PE 13-33-7 210-211cm - Average	210.5	29.51	67.71	2.78
PE 13-33-7 214-215cm - Average	214.5	12.50	46.22	41.28
PE 13-33-7 220-221cm - Average	220.5	64.36	33.53	2.11
PE 13-33-7 230-231cm - Average	230.5	69.41	28.54	2.05
PE 13-33-7 240-241cm - Average	240.5	38.96	58.71	2.33

Table A1: Grain size data for PE13-33-7 GC-5

Appendix B: Fraction mass data
(Table B1)

Depth Interval (cm)	63-150µm Fraction	150-212µm Fraction	212-355µm Fraction	>355µm Fraction	Total	Picked Mass (mg)
4	0.00487	0.00143	0.00313	0.00902	0.018	50.056
7	0.00313	0.00097	0.00175	0.00593	0.012	12.420
10	0.00210	0.00067	0.00130	0.00424	0.008	19.762
13	0.00165	0.00046	0.00114	0.00375	0.007	3.013
16	0.00254	0.00064	0.00120	0.00503	0.009	26.434
19	0.00275	0.00077	0.00168	0.00587	0.011	68.135
22	0.00161	0.00024	0.00254	0.00312	0.008	38.348
25	0.00682	0.00175	0.00301	0.00773	0.019	81.622
28	0.00190	0.00050	0.00037	0.00041	0.003	2.558
31	0.00279	0.00119	0.00264	0.00846	0.015	76.536
34	0.00277	0.00111	0.00247	0.00806	0.014	68.465
37	0.00311	0.00108	0.00232	0.00749	0.014	69.710
40	0.00375	0.00117	0.00230	0.00682	0.014	76.533
43	0.00392	0.00138	0.00293	0.00790	0.016	82.106
46	0.00444	0.00157	0.00336	0.01031	0.019	117.551
49	0.00418	0.00146	0.00308	0.00983	0.018	77.969
52	0.00400	0.00135	0.00270	0.00815	0.016	68.391
55	0.00425	0.00142	0.00396	0.01185	0.021	110.235
58.2	0.00185	0.00089	0.00213	0.00666	0.011	30.786
61	0.00152	0.00056	0.00067	0.00169	0.004	10.152
64	0.00305	0.00050	0.00075	0.00197	0.006	18.681
67	0.00499	0.00135	0.00270	0.00843	0.017	75.074
70	0.00193	0.00051	0.00135	0.00455	0.008	51.384
73	0.00210	0.00066	0.00136	0.00365	0.008	37.035
76	0.00188	0.00050	0.00126	0.00353	0.007	41.810
79	0.00330	0.00107	0.00242	0.00669	0.014	71.826
82	0.00245	0.00084	0.00209	0.00522	0.011	49.574
85	0.00209	0.00062	0.00174	0.00512	0.010	58.773
88	0.00342	0.00112	0.00288	0.00800	0.015	89.286
91	0.00395	0.00121	0.00312	0.00716	0.015	82.798
94	0.00494	0.00127	0.00287	0.00635	0.015	69.545
97	0.00919	0.00196	0.00347	0.00639	0.021	64.321
100	0.00432	0.00117	0.00331	0.00889	0.018	114.652
103	0.00397	0.00118	0.00287	0.00771	0.016	101.747
106	0.00298	0.00089	0.00191	0.00409	0.010	39.303
109	0.00742	0.00179	0.00314	0.00607	0.019	63.266

Appendix B (continued)
(Table B1)

Depth Interval (cm)	63-150µm Fraction	150-212µm Fraction	212-355µm Fraction	>355µm Fraction	Total	Picked Mass (mg)
112	0.01084	0.00186	0.00218	0.00408	0.019	39.110
115	0.00426	0.00102	0.00145	0.00345	0.010	22.229
118	0.00366	0.00126	0.00297	0.00583	0.014	62.311
121	0.00298	0.00105	0.00258	0.00519	0.012	50.293
124	0.00281	0.00088	0.00202	0.00395	0.010	47.713
127	0.00250	0.00104	0.00250	0.00478	0.011	49.002
130	0.00267	0.00091	0.00206	0.00499	0.011	59.075
133	0.00096	0.00035	0.00078	0.00144	0.004	16.881
136	0.00477	0.00149	0.00247	0.00360	0.012	37.707
139	0.00302	0.00092	0.00188	0.00346	0.009	33.306
142	0.00387	0.00134	0.00299	0.00605	0.014	62.304
145	0.00345	0.00150	0.00372	0.00785	0.017	82.215
148	0.00165	0.00061	0.00170	0.00413	0.008	33.274
151	0.00290	0.00108	0.00271	0.00728	0.014	76.689
154	0.00232	0.00088	0.00212	0.00440	0.010	43.816
157	0.00292	0.00103	0.00277	0.00597	0.013	63.180
160	0.00284	0.00096	0.00272	0.00580	0.013	58.622
163	0.00285	0.00103	0.00289	0.00658	0.013	71.879
166	0.00177	0.00062	0.00194	0.00482	0.009	44.432
169	0.00441	0.00189	0.00437	0.00717	0.018	41.050
172	0.00352	0.00162	0.00554	0.01029	0.021	78.733
175	0.00323	0.00135	0.00343	0.00697	0.015	60.121
178	0.00212	0.00094	0.00204	0.00347	0.009	38.692
181	0.00126	0.00048	0.00139	0.00257	0.006	21.224
184	0.00150	0.00043	0.00069	0.00086	0.004	6.204
188	0.00500	0.00185	0.00315	0.00563	0.016	43.458
192	0.00375	0.00142	0.00340	0.00521	0.014	46.083
195	0.00281	0.00092	0.00251	0.00461	0.011	32.307
198	0.00360	0.00134	0.00332	0.00640	0.014	53.014
201	0.00369	0.00130	0.00306	0.00574	0.014	47.501
204	0.00211	0.00080	0.00194	0.00308	0.008	30.874
207	0.00121	0.00058	0.00071	0.00104	0.003	6.017
210	0.00048	0.00008	0.00016	0.00008	0.001	1.598
213	0.00227	0.00020	0.00028	0.00032	0.003	2.269
216	0.03852	0.01272	0.01072	0.00667	0.069	28.542
219	0.00526	0.00209	0.00472	0.00824	0.020	67.493

Appendix B (continued)
(Table B1)

Depth Interval (cm)	63-150µm Fraction	150-212µm Fraction	212-355µm Fraction	>355µm Fraction	Total	Picked Mass (mg)
222	0.101	0.040	0.109	0.165	0.016	47.636
225	0.094	0.021	0.052	0.078	0.010	27.118
228	0.098	0.038	0.115	0.157	0.016	51.997
231	0.085	0.029	0.077	0.151	0.014	49.977
234	0.097	0.037	0.088	0.130	0.014	40.905
237	0.098	0.036	0.097	0.173	0.017	64.890
240	0.069	0.024	0.061	0.089	0.011	31.246
249	0.077	0.025	0.062	0.080	0.005	32.652
252	0.106	0.037	0.117	0.166	0.014	67.943
252.5	0.046	0.015	0.035	0.044	0.010	13.033
253.5	0.037	0.012	0.038	0.046	0.016	13.654
254.5	0.057	0.019	0.061	0.071	0.015	25.762
255.5	0.064	0.021	0.070	0.098	0.011	32.869
256.5	0.072	0.022	0.069	0.094	0.019	29.606
257.5	0.243	0.055	0.272	0.307	0.017	42.536
259	0.168	0.046	0.196	0.236	0.017	42.599
259.5	0.062	0.020	0.063	0.102	0.055	26.333
260.5	0.029	0.008	0.028	0.040	0.038	7.867
261.5	0.047	0.013	0.036	0.104	0.009	13.284

Table B1: Dried sieved material proportion of total wet sample mass and picked mass data.

Appendix B (continued)
(Table B2)

Depth (cm)	P. obliquiloculata (%)	N. dutertrei (%)	G. truncatulinoides (%)	G. menardii (%)	G. tumida (%)	Other (%)
4	31.7	11.4	27.7	13.1	10.0	6.0
7	63.3	4.8	19.5	5.7	5.7	1.0
10	31.5	7.6	22.3	16.9	7.0	14.6
13	28.1	8.8	40.4	1.8	8.8	12.3
16	35.2	9.2	33.2	6.3	7.6	8.6
19	26.2	8.3	23.4	21.9	8.3	12.0
22	24.3	14.2	25.9	18.8	9.4	7.4
25	18.6	7.4	37.0	17.8	10.1	9.0
28	36.8	17.5	22.8	7.0	3.5	12.3
31	38.4	15.1	27.9	6.6	6.2	5.9
34	32.7	12.7	25.8	17.7	1.7	9.4
37	17.3	8.2	30.1	19.6	17.3	7.5
40	24.1	13.9	17.3	18.3	9.9	16.4
43	31.1	8.6	12.9	12.9	11.3	23.2
46	26.2	10.2	21.3	19.1	8.0	15.2
49	22.6	8.8	20.0	22.6	10.6	15.3
52	16.7	16.2	19.8	17.7	12.3	17.2
55	19.2	16.9	14.9	16.3	10.9	21.8
58.2	26.1	20.8	14.5	11.0	11.6	16.0
61	25.3	14.1	14.1	14.7	4.1	27.6
64	15.6	12.3	16.0	15.1	3.3	37.7
67	18.6	10.5	18.0	17.0	2.3	33.7
70	18.0	13.2	24.9	25.9	2.2	15.8
73	16.3	16.9	34.5	16.9	3.9	11.4
76	18.5	17.9	25.9	20.7	3.4	13.6
79	20.9	13.8	27.9	15.1	2.1	20.1
82	17.5	18.8	24.7	14.1	2.5	22.5
85	15.3	15.3	29.8	16.9	5.5	17.2
88	11.7	16.8	24.6	17.1	3.6	26.1
91	12.1	12.4	21.2	21.8	4.9	27.7
94	11.7	19.5	25.2	12.3	9.0	22.2
97	11.1	21.3	29.3	11.6	11.1	15.6
100	7.9	15.9	21.9	7.0	10.9	36.4
103	15.3	16.9	19.6	10.8	9.3	28.0
106	15.2	17.3	15.2	11.6	18.8	22.0
109	9.4	24.2	25.5	7.6	14.2	19.1
112	16.0	28.4	21.6	10.5	13.0	10.5

Appendix B (continued)
(Table B2)

Depth (cm)	P. obliquiloculata (%)	N. dutertrei (%)	G. truncatulinoides (%)	G. menardii (%)	G. tumida (%)	Other (%)
115	16.4	24.2	21.8	17.9	10.4	9.4
118	11.0	18.2	17.6	15.4	9.1	28.6
121	9.2	15.5	15.5	23.9	4.6	31.3
124	5.3	16.3	14.1	17.6	2.2	44.5
127	12.8	28.0	12.5	20.4	7.0	19.5
130	12.1	22.5	12.7	15.4	1.6	35.6
133	15.2	24.5	14.1	11.7	2.1	32.4
136	11.4	38.7	15.7	6.3	3.1	24.8
139	10.6	29.9	10.6	5.5	1.9	41.5
142	8.1	27.7	16.5	5.5	3.5	38.7
145	16.4	26.2	13.8	8.1	4.7	30.9
148	17.4	21.6	20.3	11.1	8.5	21.0
151	8.0	22.4	14.4	15.8	3.0	36.3
154	7.0	26.9	18.0	18.0	7.3	22.8
157	9.1	27.0	11.8	13.6	5.2	33.3
160	11.0	31.5	14.5	12.7	4.3	26.0
163	6.6	24.0	13.2	12.0	6.3	37.9
166	20.3	28.5	15.9	8.2	5.3	21.8
169	12.5	43.1	15.5	10.2	5.8	12.8
172	13.6	37.4	13.9	7.0	5.1	23.0
175	10.8	36.3	10.2	18.8	4.0	20.0
178	13.6	32.0	7.6	18.4	8.2	20.1
181	13.0	34.7	17.3	13.7	9.0	12.3
184	10.7	32.8	12.3	10.7	2.5	31.1
188	8.5	30.8	13.2	3.5	6.2	37.8
192	11.1	39.6	11.6	0.2	6.6	30.8
195	12.3	39.4	9.1	2.2	6.0	30.9
198	9.4	30.2	8.6	6.9	8.6	36.3
201	13.0	34.4	9.7	0.3	12.1	30.5
204	20.7	38.1	7.7	1.1	7.7	24.7
207	4.5	27.7	7.1	11.6	6.3	42.9
210	16.7	21.4	4.8	2.4	9.5	45.2
213	3.9	37.3	2.0	0.0	3.9	52.9
216	6.2	14.2	2.2	0.0	4.3	73.2
219	10.1	27.9	2.9	0.0	16.2	42.9
222	8.5	36.0	1.8	0.0	6.1	47.6
225	10.7	33.4	7.1	0.0	8.2	40.5

Appendix B (continued)
(Table B2)

Depth (cm)	P. obliquiloculata (%)	N. dutertrei (%)	G. truncatulinoides (%)	G. menardii (%)	G. tumida (%)	Other (%)
228	7.9	34.5	4.7	0.0	9.5	43.4
231	11.2	28.7	4.8	0.0	16.6	38.7
234	9.6	34.8	6.1	0.0	14.5	35.1
237	7.5	34.2	7.8	0.0	12.9	37.5
240	11.4	27.1	6.3	0.0	14.5	40.7
243	17.1	32.7	6.3	0.0	15.6	28.3
246	9.6	33.2	4.4	0.0	16.4	36.4
249	11.8	23.6	3.3	0.0	11.2	50.2
252	5.6	29.1	3.3	0.0	16.3	45.8
252.5	2.9	24.4	2.6	0.0	8.3	61.9
253.5	8.0	21.2	6.3	0.0	16.0	48.6
254.5	9.6	20.3	2.7	0.0	11.6	55.8
255.5	12.4	22.9	3.6	0.0	21.5	39.7
256.5	11.4	17.0	3.8	0.0	16.7	51.0
257.5	22.1	23.0	1.2	0.0	34.0	19.8
259	17.9	24.5	2.5	0.0	34.8	20.4
259.5	9.6	30.5	3.0	0.0	23.2	33.8
261	8.1	33.3	4.4	0.0	21.5	32.6
261.5	13.8	22.5	2.5	0.0	13.0	48.2

Table B2: Percent abundances of >355 µm *P. obliquiloculata, N. dutertrei, G. truncatulinoides, G. menardii, G. tumida* and other species based on identification of 300 individuals if possible.

Appendix C: Radiocarbon measurement data
(Table C1)

Sample depth (cm)	Sample mass (mg)	Corrected Fm	±	Background Fm	±	Libby Age (yrs B.P.)	± (yrs B.P.)	Calibrated age (cal. yr B.P.)	Calibrated age ± (cal. yr B.P.)	Bacon chronologic weighted mean (cal. yr B.P.)
4.0	25.14	0.9465	0.0072	0.0122	0.0037	440	60	85	120	285
19.0	24.92	0.7957	0.0077	0.0134	0.0044	1840	80	1390	170	1360
25.0	25.24	0.7727	0.0082	0.0233	0.0070	2070	80	1650	210	1790
31.0	25.45	0.7614	0.0058	0.0122	0.0037	2190	60	1790	160	2120
34.0	24.88	0.7295	0.0073	0.0134	0.0044	2530	80	2200	190	2220
37.0	24.91	0.7218	0.0073	0.0134	0.0044	2620	80	2310	240	2330
40.0	25.81	0.7104	0.0070	0.0134	0.0044	2750	80	2490	240	2450
43.0	25.78	0.6974	0.0070	0.0134	0.0044	2900	80	2660	210	2550
46.0	25.16	0.7048	0.0061	0.0122	0.0037	2810	70	2560	210	2690
49.0	25.81	0.6757	0.0071	0.0134	0.0044	3150	80	2950	220	2900
52.0	25.34	0.6552	0.0068	0.0134	0.0044	3400	80	3260	210	3090
55.0	24.95	0.6469	0.0066	0.0134	0.0044	3500	80	3390	220	3270
67.0	26.05	0.6358	0.0066	0.0134	0.0044	3640	80	3550	210	3510
70.0	25.16	0.6569	0.0064	0.0122	0.0037	3380	80	3240	200	3570
76.0	25.13	0.6234	0.0064	0.0122	0.0037	3800	80	3750	220	3750
79.0	25.39	0.6095	0.0062	0.0134	0.0044	3980	80	3990	230	3850
82.0	25.18	0.6399	0.0053	0.0122	0.0037	3590	70	3490	160	3940
85.0	25.16	0.6068	0.0054	0.0122	0.0037	4010	70	4030	210	4040
88.0	25.17	0.5798	0.0073	0.0233	0.0070	4380	100	4540	290	4300
91.0	25.90	0.5726	0.0061	0.0134	0.0044	4480	90	4670	230	4490
94.0	25.18	0.5626	0.0060	0.0134	0.0044	4620	90	4850	250	4570
97.0	25.15	0.5875	0.0054	0.0122	0.0037	4270	70	4390	210	4630
100.0	25.16	0.5833	0.0053	0.0122	0.0037	4330	70	4470	210	4680

Appendix C (continued)
(Table C1)

Sample depth (cm)	Sample mass (mg)	Corrected Fm	±	Background Fm	±	Libby Age (yrs B.P.)	± (yrs B.P.)	Calibrated age (cal. yr B.P.)	Calibrated age ± (cal. yr B.P.)	Bacon chronologic weighted mean (cal. yr B.P.)
100.0	25.37	0.5499	0.0059	0.0134	0.0044	4800	90	5090	260	4680
103.0	25.14	0.5776	0.0053	0.0122	0.0037	4410	70	4580	240	4740
103.0	26.05	0.5572	0.0058	0.0134	0.0044	4700	80	4950	220	4740
106.0	25.13	0.5793	0.0054	0.0122	0.0037	4390	70	4550	230	4810
109.0	25.13	0.5575	0.0053	0.0122	0.0037	4690	80	4950	200	4910
112.0	25.17	0.5451	0.0054	0.0122	0.0037	4880	80	5180	230	5030
115.0	16.00	0.5505	0.0055	0.0122	0.0037	4800	80	5080	250	5170
118.0	25.16	0.5405	0.0055	0.0122	0.0037	4940	80	5280	300	5290
121.0	25.13	0.5361	0.0054	0.0122	0.0037	5010	80	5370	180	5420
121.0	24.34	0.5024	0.0069	0.0233	0.0070	5530	110	5920	290	5420
124.0	25.15	0.5286	0.0052	0.0122	0.0037	5120	80	5480	170	5540
127.0	25.12	0.4702	0.0052	0.0122	0.0037	6060	90	6490	210	5670
133.0	16.59	0.5280	0.0057	0.0122	0.0037	5130	90	5490	190	5850
136.0	25.14	0.5112	0.0049	0.0122	0.0037	5390	80	5770	180	5900
139.0	25.15	0.5041	0.0047	0.0122	0.0037	5500	80	5890	190	5960
142.0	25.15	0.4970	0.0051	0.0122	0.0037	5620	80	6030	200	6060
145.0	25.15	0.4901	0.0051	0.0122	0.0037	5730	80	6140	200	6190
145.0	25.29	0.4741	0.0057	0.0134	0.0044	6000	100	6420	210	6190
148.0	25.16	0.4897	0.0050	0.0122	0.0037	5740	80	6150	200	6290
151.0	25.12	0.4720	0.0052	0.0122	0.0037	6030	90	6460	210	6390
151.0	24.93	0.4566	0.0054	0.0134	0.0044	6300	100	6770	230	6390
154.0	25.11	0.5257	0.0053	0.0122	0.0037	5170	80	5530	170	6490
157.0	25.15	0.4663	0.0049	0.0122	0.0037	6130	80	6560	200	6570

Appendix C (continued)
(Table C1)

Sample depth (cm)	Sample mass (mg)	Corrected Fm	±	Background Fm	±	Libby Age (yrs B.P.)	± (yrs B.P.)	Calibrated age (cal. yr B.P.)	Calibrated age ± (cal. yr B.P.)	Bacon chronologic weighted mean (cal. yr B.P.)
160.0	25.14	0.4695	0.0053	0.0072	0.0021	6070	90	6510	210	6640
163.0	25.35	0.4331	0.0055	0.0134	0.0044	6720	100	7250	210	6760
163.0	25.16	0.4649	0.0053	0.0072	0.0021	6150	90	6590	220	6760
166.0	25.16	0.4488	0.0051	0.0072	0.0021	6440	90	6930	250	6900
169.0	25.15	0.4366	0.0051	0.0072	0.0021	6660	90	7190	220	7070
172.0	25.15	0.4307	0.0050	0.0072	0.0021	6770	90	7300	180	7170
175.0	25.17	0.4419	0.0052	0.0072	0.0021	6560	90	7080	230	7250
178.0	25.17	0.4357	0.0051	0.0072	0.0021	6670	90	7200	210	7320
181.0	19.51	0.4247	0.0049	0.0072	0.0021	6880	90	7390	170	7400
188.0	25.13	0.4144	0.0048	0.0072	0.0021	7080	90	7560	170	7640
192.0	25.12	0.4031	0.0047	0.0072	0.0021	7300	90	7770	190	7750
195.0	25.13	0.3972	0.0048	0.0072	0.0021	7420	100	7880	200	7830
198.0	25.13	0.4034	0.0051	0.0072	0.0021	7290	100	7760	200	7890
201.0	25.12	0.3900	0.0046	0.0072	0.0021	7570	100	8040	200	7950
204.0	25.11	0.3866	0.0047	0.0072	0.0021	7630	100	8100	210	8020
216.0	25.13	0.3496	0.0043	0.0072	0.0021	8440	100	9060	280	8280
219.0	25.12	0.3469	0.0051	0.0134	0.0044	8510	120	9140	300	8490
219.0	25.15	0.3662	0.0044	0.0072	0.0021	8070	100	8550	240	8490
222.0	25.11	0.3691	0.0046	0.0072	0.0021	8010	100	8480	210	8600
225.0	25.11	0.3723	0.0045	0.0072	0.0021	7940	100	8410	200	8650
228.0	25.13	0.3620	0.0045	0.0072	0.0021	8160	100	8680	310	8720
231.0	25.15	0.3684	0.0039	0.0072	0.0021	8020	80	8490	180	8810
234.0	25.12	0.3422	0.0044	0.0072	0.0021	8610	100	9270	260	8960

Appendix C (continued)
(Table C1)

Sample depth (cm)	Sample mass (mg)	Corrected Fm	±	Background Fm	±	Libby Age (yrs B.P.)	± (yrs B.P.)	Calibrated age (cal. yr B.P.)	Calibrated age ± (cal. yr B.P.)	Bacon chronologic weighted mean (cal. yr B.P.)
237.0	25.12	0.3492	0.0045	0.0072	0.0021	8450	100	9080	280	9100
240.0	25.13	0.3442	0.0045	0.0072	0.0021	8570	100	9210	270	9250
243.0	13.12	0.3301	0.0050	0.0072	0.0021	8910	120	9600	300	9410
246.0	25.15	0.3320	0.0043	0.0072	0.0021	8860	100	9530	230	9550
249.0	25.12	0.3300	0.0043	0.0072	0.0021	8910	100	9600	250	9660
252.0	25.10	0.3015	0.0049	0.0134	0.0044	9630	130	10500	340	9780
252.0	25.12	0.3193	0.0041	0.0072	0.0021	9170	100	9950	320	9780
252.5	11.87	0.3073	0.0049	0.0072	0.0021	9480	130	10350	290	9800
253.5	12.52	0.3269	0.0048	0.0072	0.0021	8980	120	9690	320	9840
254.5	23.88	0.3250	0.0041	0.0072	0.0021	9030	100	9750	310	9880
255.5	25.15	0.3269	0.0042	0.0072	0.0021	8980	100	9690	280	9910
256.5	25.12	0.3246	0.0042	0.0072	0.0021	9040	100	9760	320	9940
257.5	25.13	0.3285	0.0043	0.0072	0.0021	8940	100	9640	270	9960
258	25.12	0.3173	0.0040	0.0072	0.0021	9220	100	10000	290	9980
259.5	22.90	0.3236	0.0044	0.0072	0.0021	9060	110	9800	350	10010
261.5	12.06	0.3198	0.0049	0.0072	0.0021	9160	120	9920	360	10070

Table C1: >355 µm picked mixed foraminifera Gas Ion Source radiocarbon measurement data (ΔR = 400 years B.P., ΔR ± = 10 years B.P.)

Appendix C (continued)
(Table C2)

Sample depth (cm)	Dated material	Sample mass (mg)	Corrected Fm	±	Back-ground Fm	±	Libby Age (yrs B.P.)	± (yrs B.P.)	Calibrated age (cal. yr B.P.)	Calibrated age ± (cal. yr B.P.)	Bacon chronologic weighted mean (cal. yr B.P.)
4.0	>355µm unsorted	25.97	0.9294	0.0069	0.0138	0.0045	590	60	225	150	285
4.0	212-355µm unsorted	43.61	0.9022	0.0064	0.0138	0.0045	825	60	460	100	285
25.0	>355µm unsorted	25.25	0.7411	0.0079	0.0233	0.0070	2410	90	2050	230	1790
25.0	212-355µm unsorted	38.00	0.6812	0.0076	0.0233	0.0070	3080	90	2880	210	1790
25.0	>355µm G. truncatulinoides	23.86	0.7544	0.0083	0.0233	0.0070	2260	90	1880	220	1790
31.0	>355µm P. obliquiloculata	20.54	0.7754	0.0063	0.0138	0.0045	2040	70	1620	160	2120
55.0	212-355µm Picked	22.05	0.6439	0.0058	0.0138	0.0045	3540	70	3430	180	3270
88.0	>355µm unsorted	27.03	0.5734	0.0073	0.0233	0.0070	4470	100	4650	260	4300
88.0	212-355µm unsorted	23.07	0.5672	0.0077	0.0233	0.0070	4550	110	4750	300	4300
88.0	>355µm G. truncatulinoides	23.71	0.5669	0.0071	0.0233	0.0070	4560	100	4760	270	4300
121.0	>355µm unsorted	26.47	0.5011	0.0070	0.0233	0.0070	5550	110	5950	280	5420
121.0	212-355µm unsorted	27.94	0.5034	0.0066	0.0233	0.0070	5510	100	5900	270	5420
145.0	>355µm N. dutertrei	14.93	0.4870	0.0056	0.0138	0.0045	5780	90	6200	210	6190
145.0	212-355µm Picked	25.12	0.4910	0.0049	0.0138	0.0045	5710	80	6120	200	6190

Appendix C (continued)
(Table C2)

Sample depth (cm)	Dated material	Sample mass (mg)	Corrected Fm	±	Back-ground Fm	±	Libby Age (yrs B.P.)	± (yrs B.P.)	Calibrated age (cal. yr B.P.)	Calibrated age ± (cal. yr B.P.)	Bacon chronologic weighted mean (cal. yr B.P.)
151.0	>355µm unsorted	26.36	0.4859	0.0049	0.0138	0.0045	5800	80	6220	180	6390
151.0	212-355µm unsorted	25.33	0.4753	0.0046	0.0138	0.0045	5980	80	6400	170	6390
169.0	>355µm unsorted	26.78	0.4237	0.0048	0.0138	0.0045	6900	90	7410	170	7070
169.0	212-355µm unsorted	29.79	0.3796	0.0043	0.0138	0.0045	7780	90	8250	180	7070
172.0	>355µm N. dutertrei	25.13	0.4168	0.0045	0.0138	0.0045	7030	90	7520	150	7170
172.0	212-355µm Picked	23.11	0.4100	0.0047	0.0138	0.0045	7160	90	7640	180	7170
216.0	>355µm unsorted	27.32	0.3361	0.0047	0.0138	0.0045	8760	110	9420	240	8280
216.0	212-355µm unsorted	29.85	0.3063	0.0045	0.0138	0.0045	9500	120	10350	270	8280
216.0	212-355µm Picked	24.27	0.3333	0.0046	0.0138	0.0045	8830	110	9500	250	8280
252.0	>355µm unsorted	26.50	0.3141	0.0044	0.0138	0.0045	9300	110	10100	320	9780
252.0	212-355µm unsorted	34.99	0.3143	0.0044	0.0138	0.0045	9300	110	10100	320	9780
252.0	212-355µm Picked	24.43	0.3143	0.0046	0.0138	0.0045	9300	120	10100	330	9780

Table C2: Unsorted, 212-355 µm and >355 µm species specific Gas Ion Source radiocarbon measurement data of unsorted, 212-355 (ΔR = 400 years B.P., ΔR ± = 10 years B.P.)

Appendix C (continued)
(Table C3)

Sample depth (cm)	Sample mass (mg)	Diluent mass (mg)	Corrected Fm	±	Background Fm	±
19.0	16.80	8.20	0.8815	0.0086	0.0134	0.0044
34.0	17.23	7.75	0.8367	0.0083	0.0134	0.0044
37.0	19.01	5.93	0.8027	0.0080	0.0134	0.0044
40.0	20.07	5.03	0.7768	0.0078	0.0134	0.0044
43.0	20.40	4.52	0.7727	0.0077	0.0134	0.0044
49.0	20.11	4.75	0.7442	0.0076	0.0163	0.0054
52.0	17.56	7.69	0.7906	0.0080	0.0163	0.0054
55.0	18.12	6.83	0.7692	0.0082	0.0163	0.0054
55.0	20.79	4.14	0.7138	0.0075	0.0163	0.0054
55.0	20.30	4.78	0.7246	0.0075	0.0163	0.0054
67.0	20.36	4.65	0.7249	0.0075	0.0163	0.0054
79.0	20.70	4.30	0.6952	0.0074	0.0163	0.0054
91.0	18.79	6.26	0.6924	0.0072	0.0163	0.0054
94.0	18.76	6.27	0.6826	0.0071	0.0163	0.0054
100.0	22.51	2.50	0.6306	0.0067	0.0163	0.0054
100.0	21.26	3.81	0.6793	0.0071	0.0163	0.0054
100.0	19.19	5.97	0.6093	0.0066	0.0163	0.0054
103.0	20.38	4.64	0.6526	0.0071	0.0163	0.0054
103.0	22.69	2.34	0.5862	0.0066	0.0163	0.0054
145.0	15.79	9.12	0.6853	0.0073	0.0163	0.0054
151.0	21.31	3.75	0.5548	0.0065	0.0163	0.0054
163.0	20.36	4.69	0.5555	0.0066	0.0163	0.0054
219.0	16.94	8.06	0.5697	0.0066	0.0163	0.0054
252.0	15.78	9.17	0.5856	0.0066	0.0163	0.0054

Table C3: >355 µm picked mixed foraminifera isotope dilution Gas Ion Source radiocarbon measurement data

Appendix C (continued)
(Table C4)

Sample depth (cm)	Libby Age (yrs B.P.)	± (yrs B.P.)	Calculated Age of Sample (yrs B.P.)	Propo-gated ± (yrs B.P.)	Calibrated age (cal. yr B.P.)	Calibrated age ± (cal. yr B.P.)	Bacon chronologic weighted mean (cal. yr B.P.)
19.0	1010	80	2070	200	1660	450	1360
34.0	1430	80	2680	200	2400	490	2220
37.0	1770	80	2780	160	2510	360	2330
40.0	2030	80	2910	140	2660	350	2450
43.0	2070	80	2890	130	2630	330	2550
49.0	2370	80	3380	140	3230	360	2900
52.0	1890	80	3360	200	3220	490	3090
55.0	2110	90	3560	200	3460	490	3270
55.0	2710	80	3650	140	3570	340	3270
55.0	2590	80	3630	140	3540	350	3270
67.0	2580	80	3600	140	3510	340	3510
79.0	2920	90	3970	140	3980	390	3850
91.0	2950	80	4710	180	4980	480	4490
94.0	3070	80	4920	190	5220	470	4570
100.0	3700	90	4740	120	5010	340	4680
100.0	3110	80	4840	140	5140	360	4680
100.0	3980	90	4790	180	5070	430	4680
103.0	3430	90	4800	150	5080	390	4740
103.0	4290	90	5050	120	5400	270	4740
145.0	3040	90	6570	330	7050	690	6190
151.0	4730	90	6240	160	6700	370	6390
163.0	4720	100	6770	180	7280	370	6760
219.0	4520	90	9260	370	10050	910	8490
252.0	4300	90	10150	470	11250	1300	9780

Table C4: >355 µm picked mixed foraminifera isotope dilution Gas Ion Source radiocarbon measurement data (ΔR = 400 years B.P., ΔR ± = 10 years B.P.)

Appendix C (continued)
(Table C5)

Sample depth (cm)	Sample mass (mg)	Corrected Fm	±	Libby Age (yrs B.P.)	± (yrs B.P.)	Calibrated age (cal. yr B.P.)	Calibrated age ± (cal. yr B.P.)	Bacon chronologic weighted mean (cal. yr B.P.)
4.0	2.682	0.9185	0.0022	685	20	335	80	285
13.0	2.667	0.8715	0.0019	1110	20	670	40	670
28.0	2.458	0.7356	0.0019	2470	20	2130	100	1970
130.0	2.661	0.5031	0.0019	5520	30	5910	70	5810
184.0	5.106	0.4161	0.0016	7040	30	7530	70	7520
207.0	5.772	0.4173	0.0016	7020	30	7520	70	8060
210.0	1.318	0.4496	0.0019	6420	35	6910	110	8100
213.0	2.233	0.3866	0.0017	7640	35	8100	100	8170
257.0	2.643	0.3107	0.0019	9390	50	10230	110	9950
260.5	6.612	0.3086	0.0016	9440	40	10280	120	10050

Table C5: >355 µm picked mixed foraminifera Cesium Sputter Source radiocarbon measurement data (ΔR = 400 years B.P., ΔR ± = 10 years B.P.)

Appendix C (continued)
(Table C6)

Dated material	Corrected Fm	±	Background Fm	±	Libby Age (yrs B.P.)	± (yrs B.P.)
Standard Ref Gas	1.0398	0.0086	-	-	-310	70
C-1	0.0130	0.0005	-	-	35400	360
C-2	0.4147	0.0050	0.0131	0.0041	9150	100
CORS	1.1037	0.0090	0.0124	0.0039	-1060	70

Table C6: Gas Ion Source standard data

Appendix D: $\delta^{13}C$ and $\delta^{18}O$ stable isotope measurements data
(Table D1)

Sample depth (cm)	*T. sacculifer* $\delta^{13}C$ (‰)	*G. menardii* $\delta^{13}C$ (‰)	*T. sacculifer* $\delta^{18}O$ (‰)	*G. menardii* $\delta^{18}O$ (‰)	Calibrated age (cal. yr B.P.)	Calibrated age ± (cal. yr B.P.)	Bacon chronologic weighted mean (cal. yr B.P.)
4.0	2.359	2.398	-1.312	-0.033	85	120	285
16.0	2.275	1.624	-0.677	0.379	-	-	980
28.0	2.161	1.788	-0.57	0.469	-	-	2000
40.0	2.358	2.104	-0.712	-0.256	2490	240	2450
52.0	2.747	1.610	-0.948	0.038	3260	210	3090
64.0	-	1.989	-	0.035	-	-	3450
76.0	2.093	1.935	-1.007	0.351	3750	220	3750
88.0	2.484	1.822	-0.835	0.220	4540	290	4300
100.0	2.334	1.737	-1.299	0.759	4470	210	4680
112.0	2.291	1.523	-1.011	0.583	5180	230	5030
124.0	2.510	1.607	-1.065	0.041	5480	170	5540
136.0	2.052	1.379	-1.232	0.656	5770	180	5900
148.0	2.334	1.591	-1.048	0.400	6150	200	6290
160.0	2.214	1.531	-1.090	0.080	6510	210	6640
172.0	-	1.309	-	0.255	7300	180	7170

Table D1: $\delta^{13}C$ and $\delta^{18}O$ stable isotope measurements data of >355 µm for *T. sacculifer* and *G. menardii* and equivalent depth age data.